JOURNAL OF GEOPHYSICAL RESEARCH, VOL. 93, NO. B10, PAGES 11,877–11,897, OCTOBER 10, 1988

Intraplate Deformation and Closure of the Australia-Antarctica-Africa Plate Circuit

CHARLES DEMETS,[1] RICHARD G. GORDON, AND DONALD F. ARGUS

Department of Geological Sciences, Northwestern University, Evanston, Illinois

To determine the current motion between the Australian, Antarctic, and African plates, and to test whether this plate circuit obeys closure, all plate motion data available along the Southeast, Southwest, and Central Indian ridges are analyzed and reduced to 67 spreading rates, 38 transform fault azimuths, and 135 earthquake slip vectors. Carlsberg Ridge data were excluded because they record India-Africa, not Australia-Africa motion. New data include 10 new transform azimuths along the Southwest Indian Ridge, many slip vectors, and a dense aeromagnetic survey along the Southeast Indian Ridge. All published and many unpublished magnetic profiles are modeled to determine rates consistently over a 3-m.y. time-averaging interval for three reasons: (1) magnetic profiles from the Southeast and Central Indian ridges suggest recent spreading rate changes, (2) some published rates differ for identical profiles, and (3) prior studies have not used identical criteria and time scales to determine spreading rates. The new rates differ from published rates by as much as 5 mm/yr. Transform fault azimuths are estimated from bathymetry, Seasat altimetric data, epicenter distributions, and offsets of magnetic lineations. Azimuths of plate motion are also estimated from the horizontal projections of slip vectors from the centroid-moment tensor solutions and other focal mechanism studies. Our new Australia-Antarctica and Australia-Africa Euler vectors differ from all prior Euler vectors at the 95% confidence level. Along the Southeast and Central Indian ridges, our model gives rates differing by 4–7 mm/yr from those of prior models. From a systematic analysis of the plate motion data, we find no evidence for a Nubia-Somalia-Antarctica triple junction along the Southwest Indian Ridge. We also find no evidence for a triple junction previously proposed to be at $\sim 80^{\circ}$E along the Southeast Indian Ridge; any deformation within this seismically active region of the Australian plate adds up to less than a few millimeters per year. Along each boundary, data are fit well by a single Euler vector, except for a $\sim 5^{\circ}$ systematic misfit to azimuthal data along the eastern Southeast Indian Ridge, near a seismically active region of the Australian plate south of Tasmania. Although seismicity and the azimuthal misfit suggest the Australian plate is deforming measurably, possibly by distributed deformation or by the westward motion of a small microplate southeast of Tasmania, the significance of the misfit is marginal and is small enough that systematic errors may cause it. These alternative explanations could be distinguished by surveying these transform faults with modern seafloor mapping techniques. Prior studies found that enforcing plate circuit closure causes systematic misfits to rates along the Southeast Indian Ridge. Here we find that enforcing closure causes no systematic misfits to any data. Moreover, only insignificant nonclosure is found by an F-ratio test, which numerical experiments suggest could detect deformation exceeding ~ 2 mm/yr. We conclude that Indian Ocean plate circuit nonclosure and the deformation it suggests are much smaller than thought before. The absence of significant nonclosure argues against the usefulness of a model of deformation distributed throughout an Indo-Australian plate, but favors a model in which the significant deformation occurs in a diffuse plate boundary along the equatorial Indian Ocean between the Central Indian Ridge and the Sumatra Trench.

INTRODUCTION

Deforming lithosphere in the Indian Ocean is often cited as the type example of oceanic "intraplate" deformation. Many data suggest that near-equatorial lithosphere extending from the Central Indian Ridge to the Ninetyeast Ridge, and possibly extending farther eastward, is deforming at a rate summing to as much as 20 mm/yr. Evidence includes reverse faulting and undulations of the basement shown by reflection seismic profiling [*Eittreim and Ewing*, 1972; *Weissel et al.*, 1980; *Geller et al.*, 1983], lineated gravity and geoid anomalies that accompany the basement undulations [*McAdoo and Sandwell*, 1985; *Zuber*, 1987], heat-flow anomalies [*Geller et al.*, 1983], and large earthquakes (seven with magnitudes exceeding 7) along and near Ninetyeast and Chagos-Laccadive ridges (Figure 1*a*) [*Gutenberg and Richter*, 1954; *Sykes*, 1970; *Stein and Okal*, 1978; *Wiens and Stein*, 1984; *Bergman et al.*, 1984; *Bergman and Solomon*, 1985; *Wiens*, 1986].

Plate motion data provide indirect evidence for deformation. In a study of global plate motions, *Minster and Jordan* [1978] found that the plate motion data along the three boundaries that meet at the Indian Ocean Triple Junction are inconsistent with plate circuit closure. They attributed the nonclosure to intraplate deformation or a diffuse plate boundary that includes the Ninetyeast Ridge and possibly extends southward or southwestward to intersect the Southeast Indian Ridge. Using a new statistical test for assessing whether plate motion data justify an additional plate boundary, *Stein and Gordon* [1984] found that both *Minster and Jordan's* [1978] and *Chase's* [1978] data were fit significantly better if the Indo-Australian plate was divided into separate Indian and Australian plates by a boundary that intersects the Southeast Indian Ridge at $\sim 80^{\circ}$E, near a zone of near-ridge seismicity studied by *Bergman et al.* [1984] and *Wiens and Stein* [1984]. From new marine geophysical data near the triple junc-

[1]Now at Naval Research Laboratory, Washington, D. C.

Paper number 7B3061.
0148-0227/88/007B-3061$05.00

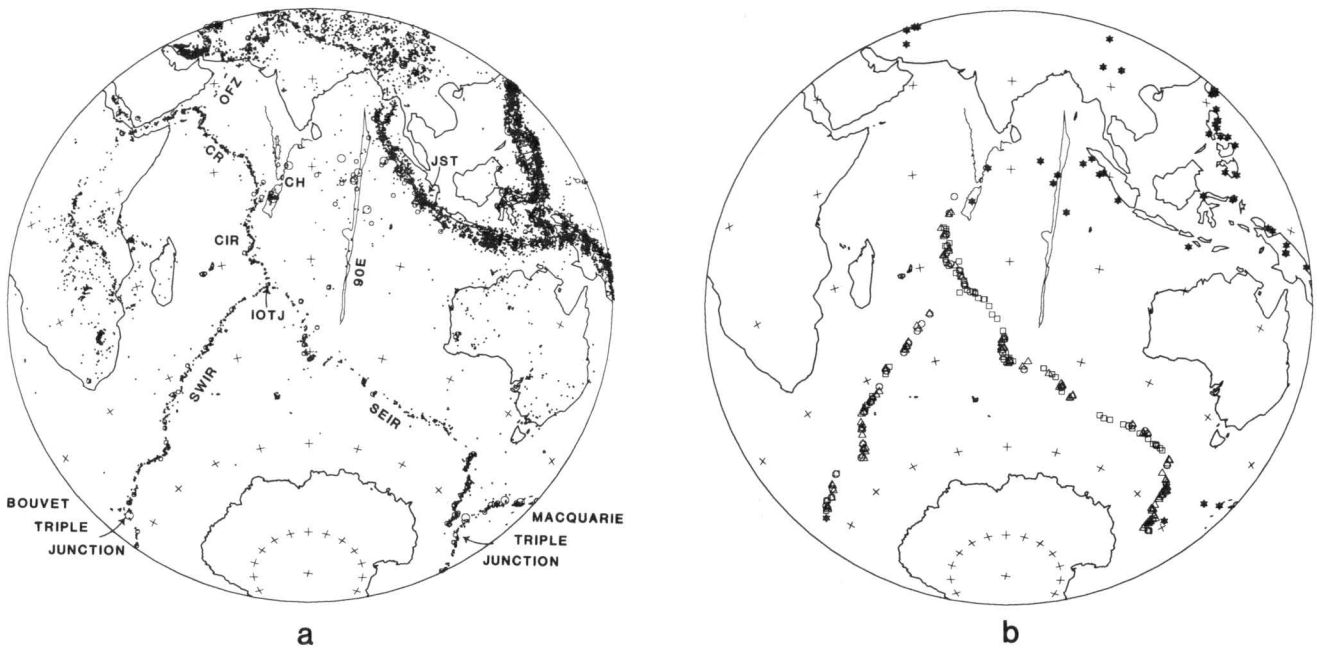

Fig. 1. (*a*) Indian Ocean location map with shallow (<50 km) seismicity from 1963 to 1985 (taken from the Earthquake Data File of the NGDC) and large historic events in the equatorial Indian Ocean. Large open circles show earthquakes with magnitudes exceeding 7.0, medium open circles show earthquakes with magnitudes between 5.5 and 7.0, and small black dots show earthquakes with magnitudes less than 5.5. Abbreviations: CIR, Central Indian Ridge; SEIR, Southeast Indian Ridge; SWIR, Southwest Indian Ridge; IOTJ, Indian Ocean Triple Junction; OFZ, Owen fracture zone; JST, Java-Sumatra Trench; CH, Chagos-Laccadive Ridge; and CR, Carlsberg Ridge. (*b*) Locations of plate motion data (Table 1). Squares show locations of seafloor spreading rates, circles show locations of transform fault azimuths, and triangles show locations of slip vector azimuths. Stars show locations of magnitude 7 or greater earthquakes, including historic events. Equal area projection.

tion, however, *Tapscott et al.* [1980] concluded that the plate circuit closes.

Since the publication of prior tests for Indian Ocean plate circuit closure, many new Indian Ocean plate motion data have accumulated (Figure 1*b*). These new data include 57 magnetic profiles across the Southeast Indian Ridge [*Vogt et al.*, 1983] (Figure 1*a*, Table 1), the azimuths of 22 transform faults, and 107 new focal mechanisms from the Harvard centroid-moment tensor (CMT) solutions [*Dziewonski and Woodhouse*, 1983; *Dziewonski et al.*, 1983*a,b*, 1984*a,b,c*, 1985*a,b,c,d*, 1986*a,b,c*, 1987*a,b,c,d,e,f,g*; *Dziewonski et al.*, 1988*a,b,c,d*] and three specialized studies [*Wald and Wallace*, 1986; *Okal and Stein*, 1987; D. Woods, personal communication, 1985].

Here we present a study of the current (0–3 Ma) motions of the Australian, Antarctic, and African plates. The goal of our study is to estimate how much these plates deform, place limits on the deformation, and investigate whether the data justify additional plate boundaries. The accurate data, well distributed along each plate boundary, strongly constrain the individual Euler vectors and allow useful tests for plate circuit closure and plate rigidity.

To catalog spreading rates as accurately as possible, we have evaluated all (~140) Indian Ocean magnetic profiles available to us, and reduced them to 67 rates well distributed along the three plate boundaries. Moreover, we have obtained digital data from the National Geophysical Data Center (NGDC) for the critical profiles near the triple junctions and all profiles available along the Central and Southeast Indian ridges. We took this time-consuming approach for three reasons: (1) to resolve discrepancies between rates published by different workers for identical profiles, (2) to minimize systematic errors caused by different criteria used to determine the "best" rate for a profile, and (3) to ensure that all rates are averaged over the same interval and referred to the same time scale, which here is the time scale of *Harland et al.* [1982]. Recent studies have shown that rates have varied by as much as 30% since 10 Ma [*Vogt et al.*, 1983]. Moreover, differences as large as 5.5% between recent and earlier time scales can cause errors of several millimeters per year along fast spreading centers such as the Southeast Indian Ridge.

Our main result is the absence of measurable nonclosure of the Australia-Antarctica-Africa plate circuit, except for possible deformation near the southeastern corner of the Australian plate. We attribute the satisfactory plate circuit closure to the new, accurate data we use and to the revised plate geometry we adopted. The consistency with plate circuit closure weakens the case for a model with significant deformation distributed throughout an Indo-Australian plate, and favors models that treat a distinct Australian plate as rigid or nearly rigid.

INDIAN OCEAN PLATE GEOMETRY

Nearly all prior studies, starting with *Wilson* [1965], adopted an Indo-Australian plate containing both India and Australia; the Indo-Australian plate separates from

TABLE 1. Australia-Antarctica-Africa Plate Motion Data

Latitude °N	Longitude °E	Datum	σ	Model	Data Importance	Ridge Azimuth	Reference
				Africa-Antarctica: Spreading Rates			
-54.70	0.00	14	3	14.7	0.088	n45w	NGDC Chain 115 leg 3
-53.90	3.50	14	3	14.8	0.086	n45w	NGDC Chain 115 leg 3
-54.00	4.00	14	4	14.8	0.048	n45w	NGDC Chain 115 leg 3
-52.20	14.50	16	3	15.1	0.085	n55w	*Norton* [1976]
-44.70	36.20	15	4	15.8	0.047	n75w	*Bergh and Norton* [1976]
-44.50	37.00	16	4	15.8	0.047	n75w	*Bergh and Norton* [1976]
-44.20	38.50	16	3	15.8	0.084	n75w	*Bergh and Norton* [1976]
-44.20	38.80	16	3	15.8	0.084	n75w	*Bergh and Norton* [1976]
-43.30	39.50	16	3	15.8	0.084	n75w	*Schlich and Patriat* [1971]
-40.00	45.60	18	4	15.7	0.047	n90w	*Fisher and Sclater* [1983]
-38.80	47.30	16	4	15.9	0.048	n80w	*Schlich and Patriat* [1971]
-26.20	68.50	16	4	15.1	0.052	n90w	*Tapscott et al.* [1980]
				Africa-Antarctica: Transform Azimuths			
-54.30	1.80	n44e	5	n46e	0.144		*Sclater et al.* [1976*a*]
-54.30	6.00	n40e	5	n42e	0.125		*Sclater et al.* [1978]
-53.50	9.00	n39e	5	n39e	0.109		*Sclater et al.* [1978]
-52.20	14.00	n36e	5	n34e	0.086		*Norton* [1976]
-53.00	25.50	n27e	15	n24e	0.007		Seasat, This study
-51.00	29.00	n25e	8	n21e	0.021		Seasat, This study
-48.00	32.00	n19e	15	n18e	0.005		Seasat, This study
-45.50	35.20	n15e	3	n15e	0.108		*Fisher and Sclater* [1983]
-44.30	38.20	n16e	10	n13e	0.009		*Bergh and Norton* [1976]
-43.80	39.30	n13e	5	n12e	0.038		*Fisher and Sclater* [1983]
-42.00	42.60	n08e	4	n10e	0.060		*Fisher and Sclater* [1983]
-39.40	46.20	n08e	3	n07e	0.121		*Fisher and Sclater* [1983]
-36.70	52.30	n04e	4	n04e	0.083		*Fisher and Sclater* [1983]
-35.70	53.30	n06e	5	n03e	0.057		*Fisher and Sclater* [1983]
-35.10	54.10	n07e	7	n03e	0.030		*Fisher and Sclater* [1983]
-33.00	57.00	n02e	3	n01e	0.195		*Sclater et al.* [1981]
-31.70	58.40	n02e	5	n01e	0.078		*Sclater et al.* [1981]
-30.00	60.80	n04w	5	n00w	0.089		*Sclater et al.* [1981]
				Africa-Antarctica: Slip Vectors			
-54.85	0.89	n51e	15	n47e	0.017		CMT *Dziewonski et al.* [1987*d*]
-54.76	1.42	n50e	20	n47e	0.009		CMT *Dziewonski et al.* [1984*c*]
-54.60	1.70	n47e	10	n46e	0.037		*Forsyth* [1975]
-54.48	2.07	n44e	15	n46e	0.016		CMT *Dziewonski et al.* [1987*e*]
-54.37	5.82	n34e	15	n42e	0.014		CMT *Dziewonski et al.* [1987*g*]
-54.40	5.90	n40e	10	n42e	0.031		CMT *Dziewonski et al.* [1987*e*]
-53.90	8.70	n47e	10	n39e	0.028		*Norton* [1976]
-53.20	9.94	n37e	20	n38e	0.006		CMT *Dziewonski et al.* [1987*a*]
-52.98	10.08	n36e	15	n38e	0.011		CMT *Dziewonski et al.* [1987*a*]
-53.35	26.10	n23e	10	n24e	0.017		*Wald and Wallace* [1986]
-52.92	26.26	n20e	10	n23e	0.016		*Wald and Wallace* [1986]
-52.48	27.99	n24e	10	n22e	0.015		*Wald and Wallace* [1986]
-52.08	28.02	n20e	10	n22e	0.015		CMT *Dziewonski et al.* [1984*a*]
-51.87	28.07	n18e	10	n22e	0.015		CMT *Dziewonski et al.* [1987*d*]
-51.84	28.23	n20e	10	n22e	0.015		*Wald and Wallace* [1986]
-51.89	28.93	n20e	15	n21e	0.006		CMT PDE (Aug. 1983)
-50.90	29.10	n26e	15	n21e	0.006		*Norton* [1976]
-48.43	31.38	n24e	15	n19e	0.005		CMT *Dziewonski et al.* [1987*f*]
-48.20	31.76	n12e	25	n18e	0.002		CMT *Dziewonski et al.* [1985*a*]
-47.67	32.54	n17e	15	n18e	0.005		CMT *Dziewonski et al.* [1987*e*]
-47.13	32.49	n15e	20	n18e	0.003		CMT *Dziewonski et al.* [1987*e*]
-45.60	34.10	n17e	15	n16e	0.004		*Norton* [1976]
-45.44	34.98	n10e	10	n15e	0.010		*Wald and Wallace* [1986]
-45.54	35.13	n18e	15	n15e	0.004		*Wald and Wallace* [1986]
-44.90	35.70	n25e	15	n15e	0.004		*Norton* [1976]

TABLE 1. (Continued)

Latitude °N	Longitude °E	Datum	σ	Model	Data Importance	Ridge Azimuth	Reference
-43.70	39.50	n08e	10	n12e	0.009		CMT *Dziewonski et al.* [1985*a*]
-43.43	40.78	n03e	10	n11e	0.009		*Wald and Wallace* [1986]
-42.96	41.96	n09e	15	n10e	0.004		CMT *Dziewonski et al.* [1987*f*]
-38.90	46.20	n14e	15	n07e	0.005		*Norton* [1976]
-39.09	46.24	n05e	20	n07e	0.003		CMT *Dziewonski et al.* [1987*g*]
-36.20	52.50	n05e	20	n03e	0.003		CMT *Dziewonski et al.* [1987*g*]
-36.44	52.85	n02e	15	n03e	0.006		CMT PDE (May 1984)
-35.69	53.41	n04e	15	n03e	0.006		CMT *Dziewonski et al.* [1986*c*]
-35.63	53.50	n05e	15	n03e	0.006		CMT *Dziewonski et al.* [1986*c*]
-34.77	54.13	n03e	15	n03e	0.007		CMT *Dziewonski et al.* [1986*c*]
-32.00	57.11	n05w	25	n01e	0.003		CMT *Dziewonski et al.* [1987*b*]
-32.64	57.48	n06e	25	n01e	0.003		CMT *Dziewonski et al.* [1988*c*]
-29.85	60.73	n05e	15	n00w	0.010		CMT *Dziewonski and Woodhouse* [1983]
-29.94	60.82	n05e	15	n00w	0.010		CMT *Dziewonski et al.* [1983*b*]
				Australia-Africa: Spreading Rates			
-12.00	66.00	37	4	35.6	0.046	n35w	*Fisher et al.* [1971]
-12.37	66.51	39	5	36.2	0.029	n35w	NGDC Chain 99 leg 5
-12.78	66.40	36	6	36.5	0.020	n35w	NGDC Circe 6
-15.52	67.00	37	10	39.4	0.007	n35w	NGDC *Conrad* 14 leg 12
-16.00	66.00	38	4	39.2	0.042	n30w	*Fisher et al.* [1971]
-18.93	65.87	42	3	42.0	0.068	n30w	NGDC Antipodes 5
-19.50	66.00	41	3	42.5	0.067	n30w	*Fisher et al.* [1971]
-19.58	68.76	46	8	44.0	0.009	n30w	NGDC *Vema* 29 leg 3
-20.30	66.50	44	4	43.5	0.037	n30w	*McKenzie and Sclater* [1971]
-21.39	68.65	45	3	45.5	0.062	n30w	NGDC *Vema* 18 leg 11
-21.57	69.00	45	4	45.8	0.035	n30w	NGDC Dodo 8
-21.95	67.96	47	3	45.6	0.062	n30w	NGDC *Vema* 20 leg 9
-23.82	69.66	51	4	48.0	0.033	n30w	NGDC Indomed leg 6
-24.43	69.63	51	5	48.5	0.021	n30w	NGDC Indomed leg 6
-24.50	69.84	50	3	48.6	0.058	n30w	NGDC Indomed leg 6
-24.77	69.80	50	4	48.9	0.032	n30w	NGDC Indomed leg 6
-24.94	69.88	50	3	49.0	0.057	n30w	NGDC *Monsoon* 4a
				Australia-Africa: Transform Azimuths			
-5.50	68.50	n45e	5	n44e	0.095		*Fisher et al.* [1971]
-9.00	67.30	n52e	3	n51e	0.224		*Engel and Fisher* [1975]
-13.50	66.50	n57e	3	n57e	0.182		*Engel and Fisher* [1975]
-16.00	66.50	n60e	5	n59e	0.059		*Fisher et al.* [1971]
-17.40	66.20	n62e	3	n61e	0.154		*Engel and Fisher* [1975]
-20.00	67.00	n60e	10	n61e	0.012		*Fisher et al.* [1971]
-22.50	69.00	n65e	15	n60e	0.005		*Fisher et al.* [1971]
				Australia-Africa: Slip Vectors			
-8.94	67.67	n40e	20	n50e	0.005		CMT *Dziewonski and Woodhouse* [1983]
-9.32	67.18	n48e	15	n52e	0.009		CMT *Dziewonski and Woodhouse* [1983]
-12.11	65.40	n52e	15	n58e	0.008		CMT *Dziewonski et al.* [1985*c*]
-13.61	65.90	n55e	20	n58e	0.004		CMT *Dziewonski and Woodhouse* [1983]
-13.68	66.29	n65e	15	n58e	0.007		D. Woods (personal communication, 1985)
-14.04	65.93	n54e	15	n59e	0.007		CMT *Dziewonski et al.* [1985*a*]
-16.58	66.77	n57e	15	n59e	0.006		CMT *Dziewonski et al.* [1986*c*]
-17.20	66.79	n56e	15	n60e	0.006		CMT *Dziewonski et al.* [1988*a*]
-17.21	66.67	n58e	15	n60e	0.006		CMT *Dziewonski et al.* [1988*b*]
-17.55	66.04	n57e	20	n61e	0.003		CMT *Dziewonski et al.* [1987*g*]
-17.97	65.36	n58e	20	n63e	0.003		CMT *Dziewonski et al.* [1988*a*]
-18.07	65.62	n57e	15	n62e	0.006		CMT *Dziewonski et al.* [1985*b*]
-19.86	66.43	n66e	15	n62e	0.006		CMT *Dziewonski et al.* [1987*b*]
-20.43	67.92	n65e	20	n60e	0.003		CMT *Dziewonski et al.* [1984*a*]
-23.01	69.26	n54e	25	n60e	0.002		CMT *Dziewonski et al.* [1987*e*]
-23.01	69.17	n48e	25	n60e	0.002		CMT *Dziewonski et al.* [1986*b*]
-23.04	69.07	n61e	25	n60e	0.002		CMT *Dziewonski et al.* [1986*b*]

TABLE 1. (Continued)

Latitude °N	Longitude °E	Datum	σ	Model	Data Importance	Ridge Azimuth	Reference
				Australia-Antarctica: Spreading Rates			
-25.81	70.23	56	3	58.0	0.066	n45w	NGDC Indomed leg 6
-26.17	71.57	57	3	58.9	0.064	n45w	NGDC Indomed leg 6
-26.37	71.96	58	3	59.3	0.063	n45w	NGDC Indomed leg 6
-26.67	72.07	59	3	59.5	0.062	n45w	NGDC Indomed leg 6
-27.70	72.70	63	4	60.4	0.034	n45w	NGDC Dodo 8
-28.00	74.00	60	10	61.2	0.005	n45w	*Sclater et al.* [1976*b*]
-28.00	74.20	61	4	61.3	0.033	n45w	NGDC *Vema* 29-03
-29.50	75.20	60	6	62.6	0.014	n45w	NGDC DSDP leg 26
-31.30	75.90	63	5	63.8	0.019	n45w	*Schlich* [1982]
-32.20	77.10	63	5	64.7	0.018	n45w	*Schlich* [1982]
-34.80	78.60	65	5	66.5	0.017	n45w	*Schlich* [1982]
-36.00	78.80	67	5	67.1	0.017	n45w	*Schlich* [1982]
-40.90	78.80	69	5	69.0	0.015	n45w	*Schlich* [1982]
-41.30	81.30	70	7	69.8	0.008	n50w	NGDC *Conrad* 11-05
-42.40	90.00	73	5	72.3	0.014	n55w	*McKenzie and Sclater* [1971]
-42.40	90.10	72	7	72.4	0.007	n55w	NGDC *Eltanin* 49
-43.50	92.60	74	10	73.1	0.003	n55w	NGDC *Eltanin* 47
-44.00	93.80	73	10	73.4	0.003	n55w	NGDC *Conrad* 8-02
-46.90	96.40	71	5	74.2	0.013	n60w	NGDC *Eltanin* 54
-49.80	110.20	73	5	75.5	0.014	n70w	NGDC *Eltanin* 49
-50.10	111.80	74	5	75.5	0.015	n70w	NGDC DSDP leg 28
-50.00	114.00	75	6	75.5	0.011	n70w	*Weissel and Hayes* [1972]
-49.80	118.70	76	2	75.1	0.101	n71w	*Vogt et al.* [1983]
-49.80	121.90	75	3	75.0	0.068	n75w	*Vogt et al.* [1983]
-50.00	125.00	76	3	74.6	0.049	n83w	*Vogt et al.* [1983]
-50.10	128.50	75	2	74.2	0.117	n83w	*Vogt et al.* [1983]
-50.40	131.00	73	2	73.8	0.123	n83w	*Vogt et al.* [1983]
-50.20	131.80	73	3	73.7	0.055	n85w	NGDC *Eltanin* 41A
-50.20	131.90	75	5	73.7	0.020	n85w	NGDC *Eltanin* 35
-50.20	132.10	73	4	73.6	0.031	n85w	NGDC *Eltanin* 41
-50.30	132.50	73	4	73.5	0.031	n85w	NGDC *Eltanin* 41
-50.30	133.90	73	3	73.2	0.057	n85w	NGDC *Eltanin* 39
-50.40	135.00	73	3	73.0	0.059	n85w	NGDC *Eltanin* 34
-52.00	140.00	72	5	71.7	0.023	s85w	NGDC *Eltanin* 36
-54.70	145.00	70	3	70.5	0.067	s80w	NGDC *Eltanin* 34
-62.50	157.80	68	4	67.5	0.040	s60w	NGDC *Eltanin* 27
-62.40	158.10	69	3	67.5	0.071	s60w	NGDC *Eltanin* 37
-62.30	158.60	68	4	67.4	0.040	s60w	NGDC *Aries* 2
				Australia-Antarctica: Transform Azimuths			
-26.20	71.00	n47e	5	n46e	0.041		*Tapscott et al.* [1980]
-36.50	79.00	n48e	15	n44e	0.004		*McKenzie and Sclater* [1971]
-39.50	78.50	n39e	15	n45e	0.003		*McKenzie and Sclater* [1971]
-41.00	80.50	n42e	15	n44e	0.003		*McKenzie and Sclater* [1971]
-43.00	84.50	n34e	15	n41e	0.003		*McKenzie and Sclater* [1971]
-46.00	96.00	n29e	15	n32e	0.003		*McKenzie and Sclater* [1971]
-49.60	120.50	n16e	4	n14e	0.039		*Vogt et al.* [1983]
-49.30	121.50	n17e	6	n13e	0.017		*Vogt et al.* [1983]
-49.00	126.10	n12e	5	n10e	0.025		*Vogt et al.* [1983]
-49.30	127.30	n11e	3	n09e	0.070		*Vogt et al.* [1983]
-52.00	140.00	n06w	10	n01w	0.007		Seasat, This study
-56.50	147.50	n13w	8	n09w	0.012		Seasat, This study
-61.50	154.50	n26w	10	n18w	0.008		Seasat, This study
				Australia-Antarctica: Slip Vectors			
-36.84	78.17	n51e	15	n45e	0.004		CMT *Dziewonski et al.* [1986*b*]
-36.65	78.68	n46e	15	n44e	0.004		CMT *Dziewonski et al.* [1987*g*]
-36.20	78.81	n51e	15	n44e	0.004		CMT *Dziewonski and Woodhouse* [1983]
-37.44	78.19	n54e	20	n45e	0.002		CMT *Dziewonski et al.* [1988*d*]
-38.35	78.05	n43e	15	n45e	0.004		CMT *Dziewonski et al.* [1986*c*]

TABLE 1. (Continued)

Latitude °N	Longitude °E	Datum	σ	Model	Data Importance	Ridge Azimuth	Reference
-38.91	78.08	n38e	15	n45e	0.004		D. Woods (personal communication, 1985)
-38.85	78.31	n45e	15	n45e	0.004		CMT *Dziewonski et al.* [1987*f*]
-38.50	78.70	n37e	15	n45e	0.003		D. Woods (personal communication, 1985)
-38.40	78.93	n45e	15	n45e	0.003		CMT *Dziewonski et al.* [1987*f*]
-40.44	78.50	n39e	10	n46e	0.008		D. Woods (personal communication, 1985)
-41.17	80.49	n30e	10	n44e	0.007		D. Woods (personal communication, 1985)
-41.31	80.52	n49e	10	n44e	0.008		D. Woods (personal communication, 1985)
-41.32	80.51	n49e	15	n44e	0.003		CMT *Dziewonski et al.* [1988*a*]
-41.63	79.66	n52e	10	n45e	0.008		CMT *Dziewonski and Woodhouse* [1983]
-41.76	80.07	n61e	10	n45e	0.007		D. Woods (personal communication, 1985)
-42.37	83.97	n25e	25	n41e	0.001		CMT *Dziewonski et al.* [1987*g*]
-41.20	85.47	n43e	20	n40e	0.002		CMT *Dziewonski et al.* [1987*g*]
-43.39	91.66	n50e	20	n35e	0.002		CMT *Dziewonski et al.* [1985*b*]
-46.09	95.41	n21e	15	n33e	0.003		CMT *Dziewonski et al.* [1985*a*]
-45.15	95.80	n59e	25	n32e	0.001		CMT *Dziewonski et al.* [1986*a*]
-45.76	96.05	n36e	15	n32e	0.003		CMT *Dziewonski et al.* [1988*c*]
-45.80	96.10	n17e	10	n32e	0.006		*Banghar and Sykes* [1969]
-45.56	96.18	n36e	15	n32e	0.003		CMT *Dziewonski et al.* [1987*g*]
-45.47	96.29	n28e	10	n32e	0.007		D. Woods (personal communication, 1985)
-47.80	99.27	n31e	15	n30e	0.003		CMT *Dziewonski and Woodhouse* [1983]
-47.87	99.42	n27e	15	n30e	0.003		CMT *Dziewonski et al.* [1987*d*]
-47.35	100.03	n33e	15	n29e	0.003		CMT *Dziewonski and Woodhouse* [1983]
-47.21	100.04	n35e	20	n29e	0.002		CMT *Dziewonski et al.* [1987*b*]
-48.96	121.27	n15e	20	n13e	0.002		CMT *Dziewonski et al.* [1987*b*]
-49.54	125.96	n16e	20	n10e	0.002		CMT *Dziewonski et al.* [1988*a*]
-49.65	125.98	n09e	15	n10e	0.003		CMT *Dziewonski et al.* [1984*b*]
-49.13	127.27	n09e	25	n09e	0.001		CMT *Dziewonski et al.* [1988*d*]
-50.95	138.99	n03w	15	n00w	0.003		CMT *Dziewonski et al.* [1987*f*]
-51.02	139.36	n00e	20	n01w	0.002		CMT *Dziewonski et al.* [1988*a*]
-51.76	139.60	n06w	20	n01w	0.002		CMT *Dziewonski et al.* [1983*a*]
-53.80	140.80	n05w	20	n03w	0.002		CMT *Dziewonski et al.* [1987*e*]
-54.17	143.80	n06w	15	n05w	0.003		CMT *Dziewonski et al.* [1984*c*]
-54.29	143.73	n05w	20	n05w	0.002		CMT *Dziewonski et al.* [1987*f*]
-54.52	144.72	n06w	15	n06w	0.003		CMT *Dziewonski et al.* [1987*d*]
-55.20	146.10	n13w	15	n08w	0.003		*Banghar and Sykes* [1969]
-55.11	146.15	n12w	15	n08w	0.003		CMT *Dziewonski et al.* [1986*c*]
-55.30	146.20	n22w	25	n08w	0.001		*Banghar and Sykes* [1969]
-54.98	146.30	n08w	15	n08w	0.003		CMT *Dziewonski et al.* [1986*b*]
-55.29	146.03	n14w	20	n08w	0.002		CMT *Dziewonski et al.* [1988*b*]
-55.53	146.41	n10w	15	n08w	0.003		CMT *Dziewonski et al.* [1985*a*]
-55.64	146.93	n05w	20	n09w	0.002		CMT *Dziewonski et al.* [1988*b*]
-56.32	146.62	n14w	20	n09w	0.002		CMT *Dziewonski et al.* [1987*e*]
-55.49	147.06	n09w	15	n09w	0.003		CMT *Dziewonski et al.* [1985*a*]
-55.49	147.42	n38w	25	n09w	0.001		CMT *Dziewonski et al.* [1988*a*]
-55.80	147.32	n12w	20	n09w	0.002		CMT *Dziewonski et al.* [1988*a*]
-55.84	147.25	n12w	20	n09w	0.002		CMT *Dziewonski et al.* [1988*a*]
-56.30	146.93	n12w	20	n09w	0.002		CMT *Dziewonski et al.* [1986*a*]
-56.57	147.33	n07w	20	n09w	0.002		CMT *Dziewonski et al.* [1987*g*]
-56.63	147.44	n13w	15	n09w	0.003		CMT *Dziewonski et al.* [1988*c*]
-56.74	147.53	n18w	15	n09w	0.003		CMT *Dziewonski et al.* [1984*c*]
-56.75	147.19	n15w	15	n09w	0.003		CMT *Dziewonski et al.* [1987*b*]
-56.83	147.32	n12w	20	n09w	0.002		CMT *Dziewonski et al.* [1987*f*]
-57.42	147.62	n14w	20	n10w	0.002		CMT *Dziewonski et al.* [1987*g*]
-57.59	148.08	n11w	15	n10w	0.003		CMT *Scott and Kanamori* [1985]
-58.94	149.11	n14w	20	n12w	0.002		CMT *Dziewonski et al.* [1988*a*]
-59.76	149.47	n19w	15	n12w	0.003		CMT *Dziewonski et al.* [1986*b*]
-59.78	150.24	n10w	15	n13w	0.003		CMT *Dziewonski and Woodhouse* [1983]
-59.63	150.29	n17w	15	n13w	0.003		CMT *Dziewonski et al.* [1987*d*]
-60.04	150.59	n17w	15	n14w	0.003		CMT *Dziewonski et al.* [1987*d*]
-60.05	152.98	n21w	15	n16w	0.004		CMT *Dziewonski et al.* [1987*c*]
-60.16	153.18	n23w	15	n16w	0.004		CMT *Dziewonski et al.* [1984*c*]
-60.17	154.71	n28w	15	n17w	0.004		CMT *Dziewonski et al.* [1988*b*]
-60.65	154.37	n22w	15	n17w	0.004		CMT *Dziewonski et al.* [1986*a*]
-61.16	153.87	n21w	20	n17w	0.002		CMT *Dziewonski et al.* [1988*c*]

TABLE 1. (Continued)

Latitude °N	Longitude °E	Datum	σ	Model	Data Importance	Ridge Azimuth	Reference
-61.27	154.37	n25w	20	n18w	0.002		CMT *Dziewonski et al.* [1987*g*]
-61.30	154.78	n24w	20	n18w	0.002		CMT *Dziewonski et al.* [1987*e*]
-61.31	154.05	n22w	20	n17w	0.002		CMT *Dziewonski et al.* [1988*a*]
-61.50	154.34	n22w	20	n18w	0.002		CMT *Dziewonski et al.* [1987*e*]
-61.67	154.95	n23w	20	n18w	0.002		CMT *Dziewonski and Woodhouse* [1983]
-61.81	154.31	n25w	15	n18w	0.004		CMT *Dziewonski et al.* [1987*b*]
-61.86	154.81	n30w	15	n18w	0.004		CMT *Dziewonski et al.* [1983*a*]
-62.51	155.02	n26w	15	n19w	0.004		CMT *Dziewonski et al.* [1987*a*]
-62.95	155.77	n24w	20	n20w	0.002		CMT *Dziewonski et al.* [1988*d*]
-63.09	155.72	n23w	15	n20w	0.004		CMT *Dziewonski et al.* [1986*a*]

A "data importance" is a measure of the information content of a datum, as defined by *Minster et al.* [1974]. "σ" is the standard error assigned to a datum. Rates and their standard errors are listed in millimeters per year. Azimuths and their standard errors are listed in degrees. All rates were determined by comparison of observed profiles to synthetic magnetic anomaly profiles that we computed. Rates determined from data we obtained from the National Geophysical Data Center data are referenced NGDC. Slip vectors referenced as CMT are determined from centroid-moment tensor solutions.

the African plate along the Central Indian and Carlsberg ridges (Figure 2*a*). Here we focus on an alternative plate geometry, in which Australia and India are on separate plates divided by a diffuse boundary in the equatorial Indian Ocean (Figure 2*b*) [*Wiens et al.*, 1985]. The Central Indian Ridge divides the African plate from the plate containing Australia, and the Carlsberg Ridge divides the African plate from the plate containing India. *Wiens et al.* [1985] presented seismological and plate motion data supporting the latter geometry and found that the nonclosure of the plate circuit about the Indian Ocean Triple Junction was reduced when their new geometry was used, although significant nonclosure remained. Because this remanent nonclosure suggests that one or more of the plates was deforming, it detracts from the usefulness of a model in which Indian Ocean lithospheric deformation occurs in a diffuse plate boundary. As will be shown here, however, our new data are consistent with plate circuit closure.

We will also assume that motion between Nubia (West Africa) and Somalia (East Africa) can be neglected near the Southwest Indian Ridge. The slow extension across the East African Rift system shows that Africa is deforming (Figure 1*a*). Both geologic and plate motion studies suggest that rifting between Nubia and Somalia decreases from north to south until the morphologic trace of the boundary and most seismicity vanishes. Our approach here is to use the plate motion data along the Southwest Indian Ridge to test whether a single-plate model for Africa is acceptable for our analysis. As will be shown, the plate motion data along the Southwest Indian Ridge are consistent with no motion between Nubia and Somalia.

Methods of Analysis and Sources of Data

Plate motion data are analyzed here on three separate tiers. At the lowest tier we analyze magnetic, bathy-

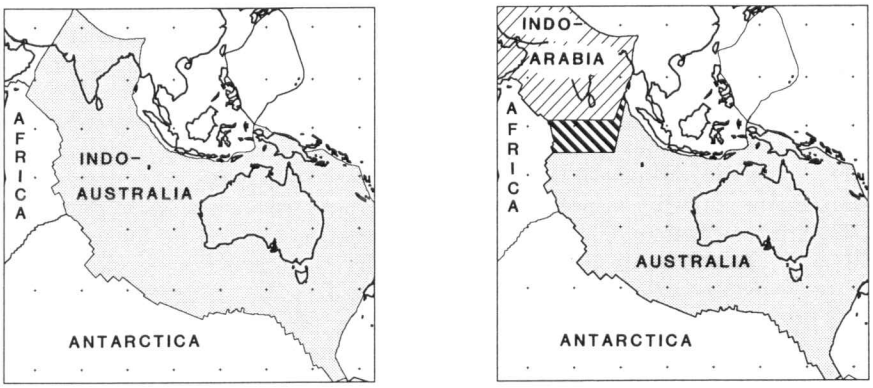

Fig. 2. (a) Geometry of the Indo-Australian plate. (b) Revised geometry of *Wiens et al.* [1985]. The Indo-Australian plate has been divided into Indo-Arabian and Australian plates. These two plates are separated by a (hachured) diffuse boundary.

metric, and other profiles to determine spreading rates and transform fault azimuths, and their associated confidence limits. We also evaluate slip vectors from focal mechanisms determined by others and estimate their associated confidence limits. At the middle tier we analyze plate motion data along a single plate boundary, find best fit Euler vectors, examine the internal consistency of data, and compare the results with those of prior studies. At the highest tier we find Euler vectors for three separate plate boundaries simultaneously, and test whether the data are consistent with plate circuit closure. Below we describe the methods of analysis adopted for each tier.

Lowest Tier: Spreading Rates, Transform Azimuths, and Slip Vectors

We used three types of plate motion data: spreading rates from marine magnetic profiles, azimuths of transform faults, and slip vectors derived from earthquake focal mechanisms. The data include 38 transform fault azimuths, 135 earthquake slip vectors, and 67 spreading rates derived from 93 useful marine magnetic profiles selected from the ~140 profiles we examined (Table 1, Figure 1b). When assigning an error to each datum, we tried to be consistent with errors assigned in prior studies. As was the case in prior studies, the assigned errors probably are systematically too large.

Spreading rates. For each magnetic profile we used standard techniques [*Schouten and McCamy*, 1972] to generate a series of synthetic magnetic profiles differing by 1 mm/yr in full spreading rate (e.g., Figure 3). The synthetic profile that best fit the observed profile at the center of the anomaly 2′ sequence (2.92–3.15 Ma) gave the rate we adopted. For the fast spreading Southeast Indian and Central Indian ridges, all but one profile showed the characteristic 2′ double peak on both sides of the ridge. Anomaly 2′ also appeared on both sides of the ridge for all Southwest Indian Ridge profiles, but the slow spreading rate caused the two peaks to merge (Figure 4). Rates are determined either from the best fit to an individual profile, or from averaging the best fit rates from several, closely spaced profiles (Table 1).

The errors assigned to spreading rates depended on the number of profiles averaged to obtain a rate, the reproducibility of rates when different co-authors examined the same profile, the subjectively estimated precision with which we could determine the rate from an individual profile, and how far the ship track departed from the ridge-normal direction. The error assigned to an individual profile ranged from 3 mm/yr for profiles with a complete, easily identified sequence of anomalies through 2′, to 10 mm/yr for profiles with an incomplete sequence, tenuous anomaly identifications, or with suspected ridge jumps. On 75 of the 93 useful magnetic profiles, we could identify the Central and Jaramillo anomalies, and anomalies 2 and 2′; rates determined from good profiles were assigned errors of 3 or 4 mm/yr. The narrow 3 to 4 mm/yr range of assigned errors applies to a wide range of spreading rates (14–76 mm/yr). As spreading rates increase, so does the resolvability of individual anomalies. Fast spreading (≥60 mm/yr) produces good anomalies that resolve features produced from seafloor formed during brief chrons (Figure 3). Slow spreading (~15 mm/yr) typically produces poor anomalies with low resolution of the center of anomaly 2′ (Figure 4).

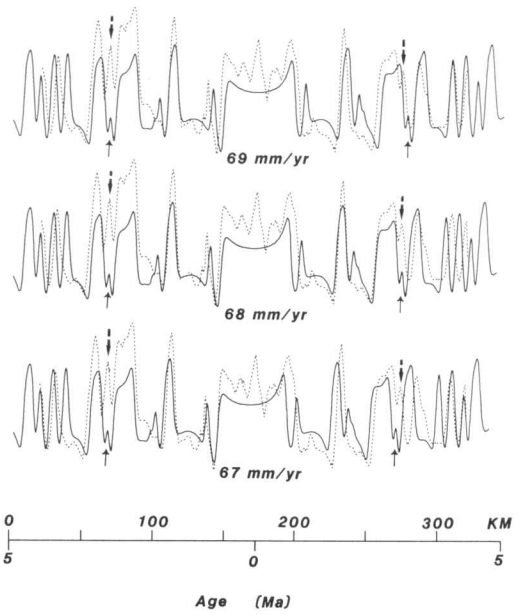

Fig. 3. Comparison of an observed *Eltanin* 27 magnetic profile (dashed curves) from the NGDC to synthetic magnetic anomaly profiles (solid curves) computed for rates of 67, 68, and 69 mm/yr. The profile crosses the Southeast Indian Ridge at 158° E (near the Macquarie Triple Junction). The 3.0-Ma center of the anomaly 2′ sequence (marked by arrows) is aligned on the left-hand side of each profile. The synthetic profile at 69 mm/yr is too fast, and the synthetic profile at 67 mm/yr is too slow, showing that the 68 mm/yr rate can be determined with a precision of 1 mm/yr. This profile has already been projected onto a ridge-normal direction.

Smaller errors were assigned to five rates determined from averages of several closely spaced profiles. Closely spaced profiles allow fracture zones and propagating rifts to be identified, eliminating two sources of error on isolated profiles. Averaging rates from closely spaced profiles reduces the error of the mean rate for a group of profiles; a mean rate from several profiles is thus typically assigned a smaller error than is a rate from an isolated profile. Although the formal confidence limits of these averages were 1 mm/yr or less, we arbitrarily adopted a floor of 2 mm/yr for the smallest error we assigned. Our intent is to allow for possible systematic errors, which include wrong correlation of anomalies because of unrecognized fracture zones or propagating rifts, sloping reversal boundaries, or limitations of the simple, single-layered, two-dimensional block model we used to compute synthetic anomalies.

Transform azimuths. Transform fault azimuths were estimated from bathymetry, Seasat altimetry, alignment of earthquake epicenters, and offsets of magnetic lineations. We used several criteria for choosing transforms and calibrating their standard errors. We excluded transforms with offsets less than 30 km because studies of Mid-Atlantic Ridge transforms show that short-offset transforms do not parallel plate motions [*Searle and Laughton*, 1977; *Collette et al.*, 1979; *Rona and Gray*, 1980; *Macdonald*, 1986; *Searle*, 1986]. Errors assigned to transform trends were based on subjective estimates of the accuracy of the data (Table 1). For azimuths constrained by bathymetry, the assigned error depended on the

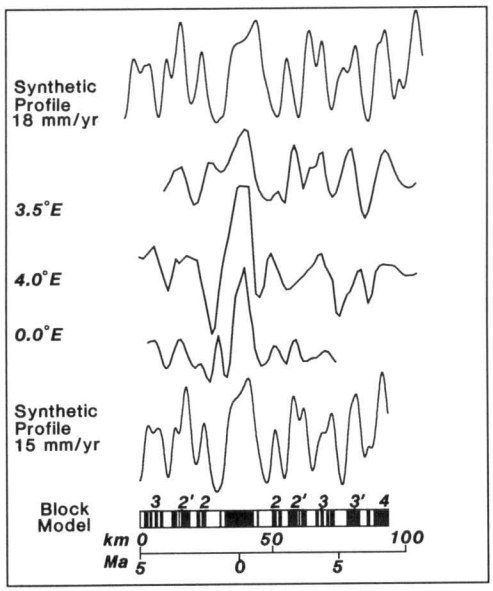

Fig. 4. Chain 115, leg 3 magnetic anomaly profiles (from the NGDC) from 0 to 4° E along the Southwest Indian Ridge. The 15-mm/yr synthetic profile best fits the three observed profiles, but a rate of 18 mm/yr (top) cannot be excluded. Profiles are shown along track; ridge-normal rates determined by projecting the rate for each profile onto the ridge-normal trend are 17 mm/yr (top) and 14 mm/yr (bottom).

number of ship track crossings of the transform. Transforms with only two or three crossings were usually assigned 10–15° errors; transforms with five or more crossings were assigned errors of 3–5°, depending on the density and distribution of the ship track crossings, and the linearity of the transform valley. Four otherwise poorly constrained transform azimuths were estimated from Seasat profiles on GEBCO chart overlays [*Sandwell*, 1984]. Lithospheric age offsets across transforms and fracture zones produce characteristic signatures in the geoid [*Sandwell*, 1984]. On along-track first derivatives of Seasat altimetric data, the signature depends on the direction of satellite approach: transforms (or fracture zones) approached from the older side give a peak, whereas transforms approached from the younger side give a trough. We used no tracks crossing near the midpoint of a transform because the age offset is small. Because fracture zone trends help locate the endpoints of transforms, we also determined locations of fracture zone crossings. The locations from the Seasat data, shown along the flight tracks, agree well with available bathymetry and with epicenter locations from the National Geophysical Data Center's Earthquake Data File (Figures 5 and 15). Errors assigned to transform trends determined from Seasat data were 8° or larger because these data may not resolve small ridge offsets that could bias the measured trend. For instance, a short ridge offset near 52°S, 140°E (Figure 15) is not apparent from Seasat data or the distribution of epicenters, but is seen in bathymetric and magnetic data. Four transform trends were determined from offset magnetic lineations observed on closely spaced aeromagnetic profiles [*Vogt et al.*, 1983]; their errors were determined from the locations of the profiles.

Slip vectors. Slip vectors were used from CMT solutions [e.g., *Dziewonski et al.*, 1983*a*,*b*] and from many other sources (Table 1). We avoided slip vectors from earthquakes near ridge-transform intersections. We used earthquakes with moments as low as 10^{23} dyn cm. The 15° error assigned to many (68 of 135) slip vectors is intended to reflect both instrumental and experimental errors, and equals the largest error assigned to transform azimuths. Slip vectors determined from focal mechanisms with poor first-motion data or moments less than 10^{25} dyn cm were assigned higher errors, 20° and 25°. Twelve slip vectors determined from both first-motion and body wave modeling were assigned 10° errors.

Middle Tier: Euler Vectors and Consistency of Data from a Single Plate Boundary

We determine best fitting Euler vectors with a weighted least squares algorithm based on *Chase's* [1972] fitting functions. The functions are linear in rate but nonlinear in azimuths and slip vectors. We linearize the fitting functions about a trial solution and solve for parameter increments iteratively until the solution converges. Chase's formulation for rates fits the projection of the surface velocity vector onto the horizontal ridge-normal direction; thus observed rates must be ridge-normal. This differs from *Minster and Jordan's* [1978] analysis where observed rates are measured parallel to an assumed direction of relative motion. Here, neither approach offers an important advantage over the other, except that our program based on

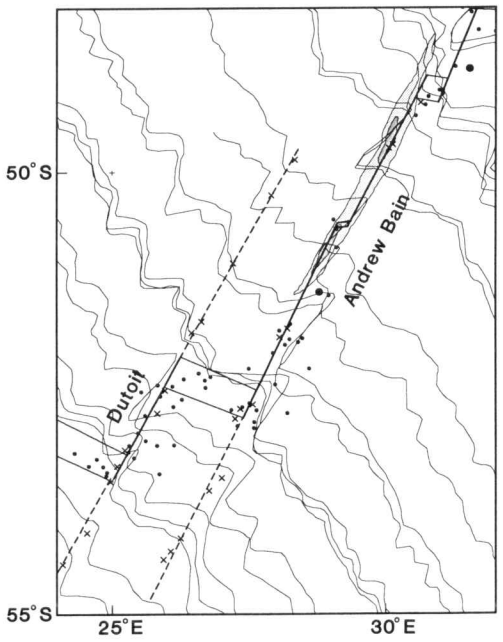

Fig. 5. Data limiting the trend of the Andrew Bain transform fault, a 480 km offset of the Southwest Indian Ridge. The along-track deflections of the vertical for ascending Seasat altimeter passes [*Sandwell*, 1984] are used to locate the fracture zone and transform fault. Small crosses mark the fracture zone (dashed line) or transform fault (solid line) identifications projected onto the track lines. Transform valley 4500- and 5000-m depth contours from *Falconer and Tharp* [1981] are shaded. The locations of the ridge segments are unconstrained by bathymetric data but are inferred from transform fault offsets and earthquake epicenters.

Chase's formulation runs 6 to 8 times faster than our program based on Minster and Jordan's formulation.

Euler vector confidence limits are determined by linear propagation of errors. To compare the standard error confidence ellipse determined by *Minster and Jordan* [1978] to those we give here, Minster and Jordan's errors must be multiplied by $2^{1/2}$ because they describe one-dimensional standard errors, whereas here we give standard errors appropriate for two dimensions (cf., figures 3 and 4 of *Cox and Gordon* [1984].

To test the internal consistency of data from each individual plate boundary, we applied a statistical test for additional plate boundaries [*Stein and Gordon*, 1984], which is useful for locating plate boundaries poorly defined by seismicity and bathymetry, or for identifying systematic data biases. The test assumes that data from a boundary should be fit well by a single Euler vector if both plates are rigid. If the same data are split into two subsets at a hypothetical triple junction along the boundary, and the two resulting subsets of data are each fit by its own Euler vector, the misfit decreases. We use an F-ratio test to determine whether the decrease is significantly greater than expected solely from introducing more adjustable parameters. An F value exceeding that expected at the 1% risk level suggests that an additional plate boundary intersects the boundary being analyzed, or that some data along a boundary have systematic errors. This test is repeated for every possible hypothetical triple junction location along a single plate boundary. Our method here differs slightly from that of *Stein and Gordon* [1984], who assumed that only three adjustable parameters (the three components of an Euler vector) are added when testing for a hypothetical triple junction. The location of the triple junction along the known plate boundary is also an adjustable parameter, which is why we use an F-ratio test of 4 versus N-7 degrees of freedom here, not 3 versus N-6 degrees of freedom as used before.

Upper Tier: Three-Plate Models and Plate Circuit Closure

We determine a three-plate model that enforces plate circuit closure using standard extensions of methods for determining an Euler vector for a single pair of plates. Methods of inverting the data from three or more plate boundaries have been described before by *Chase* [1972] and *Minster et al.* [1974]. We assess triple junction closure with a recently proposed F-ratio test of plate circuit closure, which focuses on the differences in the overall fit to the data of two different models. One model consists of three Euler vectors found by fitting all data while enforcing closure. Only six independent parameters are determined from the data. The second model consists of three Euler vectors derived by fitting the data along each plate boundary separately. Because closure is not enforced, nine independent parameters are determined [*Gordon et al.*, 1987].

The test is formulated using χ^2, the total weighted least squares misfit, and is analogous to the test of additional terms widely used in curve fitting. The value of χ^2 determined with nine adjustable parameters (N-9 degrees of freedom) is always less than the value of χ^2 determined from the same data but with only six adjustable parameters (N-6 degrees of freedom). To test if the reduction in χ^2 is greater than would be expected merely because more model parameters were added, the statistic

$$F_{3,\,N-9} = \frac{\left(\chi^2(6) - \chi^2(9)\right) / 3}{\chi^2(9) / (N-9)} \tag{1}$$

is used. This statistic is expected to be F distributed with 3 versus N-9 degrees of freedom [*Bevington*, 1969]. The experimentally determined value of F is compared with a reference value from standard tables [e.g., *Spiegel*, 1975] of $F_{3,\,N-9}$ with less than a 1% probability of being exceeded by chance. If the experimental value exceeds the reference value, then there is a 99% probability that the plate circuit fails closure.

Results of Analysis Along Individual Plate Boundaries

Southwest Indian Ridge

Along the Southwest Indian Ridge, observed rates are 14–18 mm/yr (Figure 6), similar to those used by *Minster and Jordan* [1978] and *Tapscott et al.* [1980], but slower than the 20 mm/yr rate used by *Chase* [1978]. The 16-mm/yr rate determined from *Tapscott et al.'s* [1980] profile is important because it extends rate coverage far eastward of rates available to *Minster and Jordan* [1978] and *Chase* [1978]. From NGDC data, we estimated the rate near the Bouvet Triple Junction to be 14 mm/yr, about the same as found by *Sclater et al.* [1976*a*] from the same data. The sequence of anomalies across this slow spreading center is poorly developed, however, and we doubt 14 mm/yr is a significantly better fit than several alternative rates, such as 17 mm/yr (Figure 4).

We use 18 transform azimuths along the Southwest Indian Ridge. Ten of the many long-offset transforms along the Southwest Indian Ridge have been recently surveyed [*Sclater et al.*, 1981; *Fisher and Sclater*, 1983]. Because of poor bathymetric control along the Du Toit (25°E), Andrew Bain, and 32°E transforms, we measured their trends from Seasat data [*Sandwell*, 1984] and checked them with locations of earthquake epicenters (Figure 5), and found trends similar to those estimated by *Wald* [1986]. We determined the trend of only the southern half of the Andrew Bain transform because the bend in the middle of the transform may be a small spreading ridge segment or extensional relay zone [*Wald and Wallace*, 1986; *Royer et al.*, 1986; *Okal and Stein*, 1987], as is also suggested along the 32°E transform by two normal faulting earthquakes [*Wald and Wallace*, 1986]. Our data include more than twice as many transform azimuths as prior data sets. Thirty-nine slip vectors from many sources further limit the direction of plate motion (Table 1).

Our best fitting Euler vector is similar to Euler vectors determined by *Minster and Jordan* [1978] and *Tapscott et al.* [1980] (Figures 6 and 20), but differs from that of *Chase* [1978]. Because the southern continuation of the East African Rift system, if it exists, may intersect the Southwest Indian Ridge, we tested the plate motion data for systematic misfits using the method of *Stein and Gordon* [1984]. The improved distribution and increase in the number of plate motion data give a strong test for relative motion, which presumably is slow because the boundary

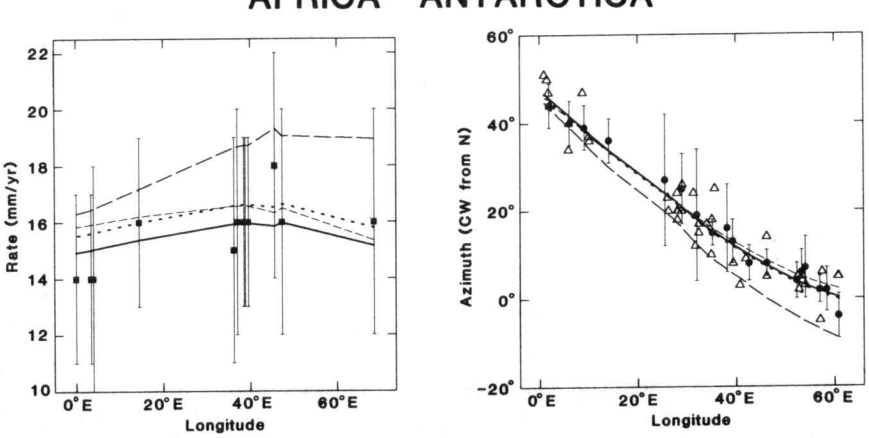

Fig. 6. Africa-Antarctica plate motion data observed along the Southwest Indian Ridge are compared to rates and azimuths calculated from different plate motion models. Squares show seafloor spreading rates determined from surface magnetic profiles, circles show observed transform fault azimuths, and triangles show observed slip vector azimuths. The solid line was calculated from our best fitting vector, the long-dashed line from *Chase's* [1978] model, the medium-dashed line from *Minster and Jordan's* [1978] RM2 model, and the short-dashed line from *Tapscott et al.'s* [1980] model.

has only a weak seismic expression and no morphologic expression in the seafloor south of Africa. The lack of significant reduction in misfit, regardless of the location of a hypothetical Nubia-Somalia boundary (Figure 7), suggests that little, if any, Nubia-Somalia motion occurs near the Southwest Indian Ridge, a conclusion supported by the agreement between the model and the observed rates and azimuths (Figure 21). The internal consistency of these data suggests they give motion along a single boundary and can thus be included in the analysis of the closure of the Africa-Antarctica-Australia plate circuit.

Central Indian Ridge

Only three useful magnetic profiles, which are near the Indian Ocean Triple Junction, have been published since 1975 [*Tapscott et al.*, 1980]. Because Central Indian Ridge rates are critical for assessing closure of the plate circuit, we analyzed all magnetic profiles south of 5°S available from the NGDC. Thirteen of the 22 profiles gave useful rates. Four more rates were determined from published profiles unavailable from the NGDC. Profiles from 25 to 19°S give spreading rates that decrease from ~50 mm/yr to ~42 mm/yr (Figure 8). Seventeen slip vectors fill a former gap in azimuth data along the Central Indian Ridge.

The best fitting vector fits both the rates and azimuths well (Figure 9). The statistical test for additional plate boundaries also finds no systematic misfits (Figure 10).

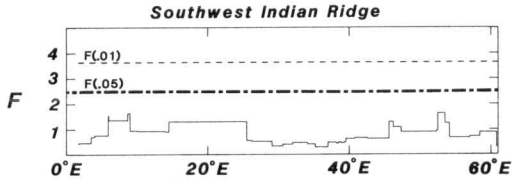

Fig. 7. F versus hypothetical triple junction locations along the Southwest Indian Ridge. The dashed line is the threshold for the 1% risk level and the dot-dashed line is the threshold for the 5% risk level. If any part of the curve exceeded either reference line, we would conclude that the data are fit significantly better by assuming the Nubia-Somalia plate boundary intersects the Southwest Indian Ridge at that point. Because the curve never exceeds either reference line, we conclude that any Nubia-Somalia motion is meager, widely distributed, or both.

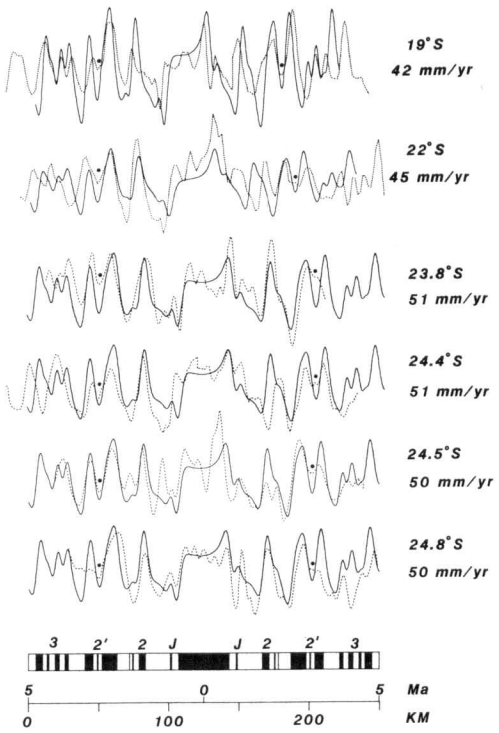

Fig. 8. Observed magnetic profiles (dashed curves) along the Central Indian Ridge compared to best fitting synthetic magnetic anomaly profiles (solid curves). The observed profiles, which were obtained from the NGDC and projected onto the ridge-normal direction, record rates that decrease northward. The observed rates are systematically slower than expected from *Minster and Jordan's* [1978] RM2 model.

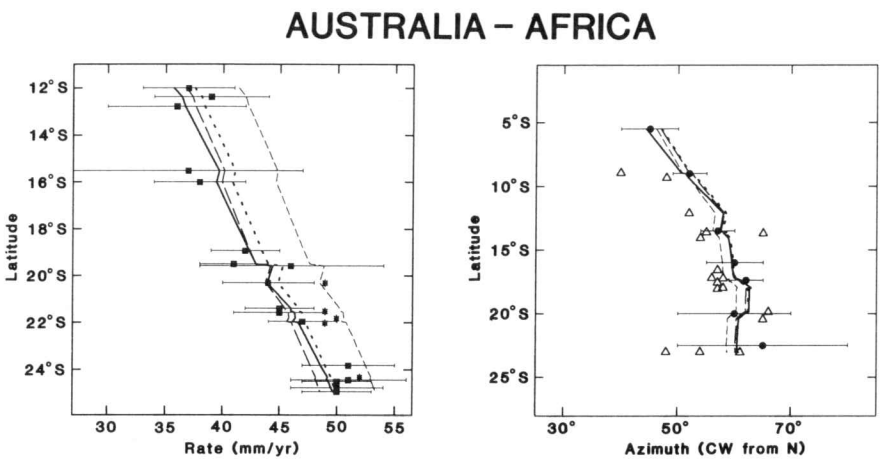

Fig. 9. Australia-Africa plate motion data observed along the Central Indian Ridge are compared to rates and azimuths calculated from different plate motion models. Squares show seafloor spreading rates determined from surface magnetic profiles, circles show observed transform fault azimuths, and triangles show observed slip vector azimuths. The solid line was calculated from our best fitting vector, the long-dashed line from *Chase's* [1978] model, the medium-dashed line from *Minster and Jordan's* [1978] RM2 model, and the short-dashed line from *Tapscott et al.'s* [1980] model. The rates used by *Minster and Jordan* [1978] are shown by asterisks.

Prior Euler vectors give similar fits to the azimuths, and two prior models give similar fits to the rates (Figure 9).

However, the *Minster and Jordan* [1978] Euler vector predicts rates higher than we adopt (Figure 9). For example, four profiles that cross the Central Indian Ridge between 20°S and 25°S give rates of 50-51 mm/yr for the southernmost profiles and 42–45 mm/yr for the northernmost profiles (Figure 8). The rates we determined are similar to those estimated by *McKenzie and Sclater* [1971], *Chase* [1978], and *Tapscott et al.* [1980]. *Minster and Jordan's* [1978] model predicts rates of ~53 mm/yr for the southernmost four profiles and ~50 mm/yr for the northerly profiles. The magnetic profiles seem good enough to exclude rates as fast as those previously predicted.

Southeast Indian Ridge

The Southeast Indian Ridge has more plate motion data than the other Indian Ocean boundaries. The spreading rates near its ends, the Macquarie and Indian Ocean triple junctions, are accurately determined. Near the Indian Ocean Triple Junction, four good magnetic profiles establish the rate and suggest that it increases eastward (Figure 11). Allowing for differences between magnetic reversal time scales, the rates we determined from profiles near the Indian Ocean Triple Junction are similar to those determined by *Tapscott et al.* [1980]. Bathymetry near the Indian Ocean Triple Junction constrains the trends of transform faults to be N47±5°E [*Tapscott et al.*, 1980]. Near the Macquarie (Australia-Pacific-Antarctic) Triple Junction, the spreading rate is recorded by four profiles, three of which are shown in Figure 12. Each profile has easily recognized and correlatable anomalies that establish the ridge-normal spreading rate to be ~68 mm/yr, slightly faster than found by *Falconer* [1972].

The most detailed survey of spreading rates in the Indian Ocean consists of 57 ridge-normal aeromagnetic profiles between 115°E and 132°E along the Southeast Indian Ridge [*Vogt et al.*, 1983]. This survey, unavailable to prior plate motion studies, accurately establishes the rate to be faster than predicted by prior models (Figures

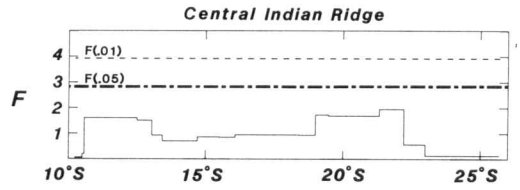

Fig. 10. F versus hypothetical triple junction locations along the Central Indian Ridge. The dashed line is the threshold for the 1% risk level, and the dot-dashed line is the threshold for the 5% risk level.

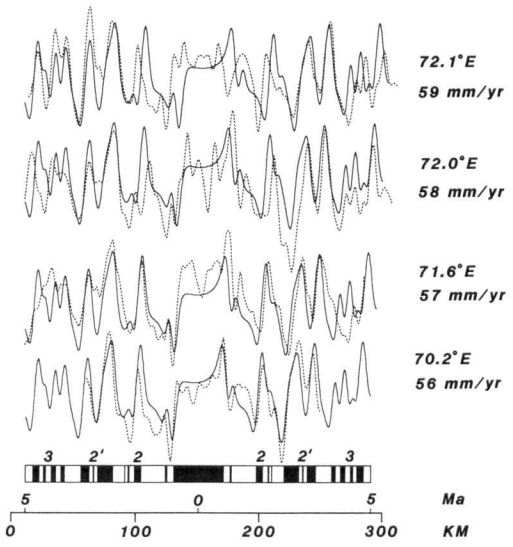

Fig. 11. Along-track Southeast Indian Ridge NGDC magnetic anomaly profiles near the Indian Ocean Triple Junction. Each observed profile (dashed curves) shows anomaly 2′ on both sides of the ridge. The synthetic profiles (solid curves) were computed assuming a constant spreading rate shown to the right of each profile.

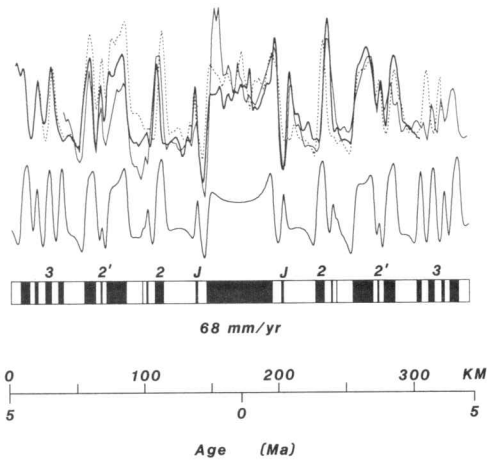

Fig. 12. Magnetic anomaly profiles near the Macquarie Triple Junction. These NGDC profiles include *Eltanin* 37 (bold solid), *Eltanin* 27 (dashed), and Aries 02 (thin solid); they give the easternmost rate observed along the Southeast Indian Ridge. The lower profile is a model computed for a 68-mm/yr rate, which is the 3-m.y. average rate that fits two of three of these profiles best (Table 1).

13 and 16). From the best 30 of these 57 closely spaced profiles, we determined a rate for each profile and then determined the mean rate for each of five profile groups. Surface magnetic profiles between 90°E and 110°E (e.g., top three profiles in Figure 14) give rates consistent with

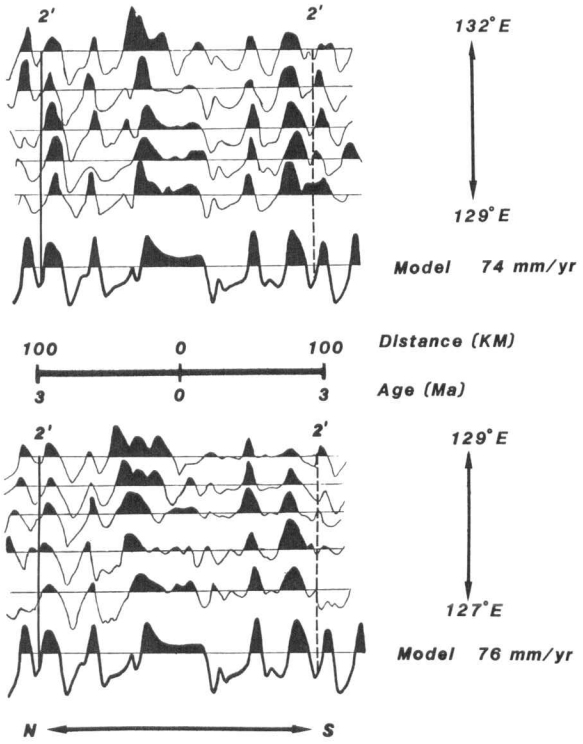

Fig. 13. Aeromagnetic profiles along the Southeast Indian Ridge [Vogt et al., 1983] compared with 74- and 76-mm/yr synthetic magnetic profiles. Anomaly 2′ is connected on the left (north) by a solid line; the dashed line shows where the center of 2′ would be on the right (south) for a perfect fit. These closely spaced aeromagnetic profiles give rates that exclude the slower rates predicted by prior models.

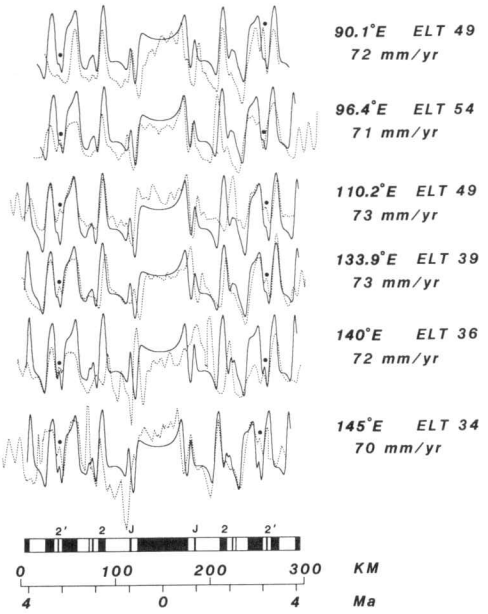

Fig. 14. Along-track Southeast Indian Ridge NGDC magnetic anomaly profiles, 90–145° E. The center of anomaly 2′ for each observed (dashed) profile is marked with a solid circle. The synthetic profile (solid) that best fits the center of anomaly 2′ for each observed profile is also shown. The profiles have been projected onto ridge-normal directions listed in Table 1.

older models, but surface profiles east of 130°E (e.g., bottom three profiles in Figure 14) give rates systematically faster than predicted by older models (Figure 16).

In the sparsely surveyed 135–155°E region, at least six transform faults offset the ridge (Figure 15); bathymetry weakly defines their trends and suggests the basement morphology is complex [*Hayes and Conolly*, 1972]. We used earthquake epicenter locations and magnetic and bathymetric data to locate these transforms and transform fault signatures of the descending Seasat altimeter passes to estimate the trends of three of these transforms. Forty-seven slip vectors, only two of which were used in prior plate motion studies, give the azimuth of motion along these six transforms (Figure 15).

The best fitting vector fits the well-distributed high-quality rates well. However, the azimuths show a small but systematic misfit: the observed azimuths tend to be ~2° clockwise of the azimuths calculated from the best fitting Euler vector near 120°E, and ~5° counterclockwise of the model azimuths near 140–150°E (Figures 16 and 23). Azimuth predictions of prior Euler vectors are similar to ours and show the same small systematic misfit to the observed azimuths. However, the new model gives faster rates than given by prior models east of 115°E (Figure 16). Moreover, the models of *Chase* [1978] and *Minster and Jordan* [1978] predict rates too fast west of 90°E. The profiles west of 90°E seem good enough to exclude the fast rates predicted by these two prior models (Figure 11). Australian-Antarctic Discordance profiles seem good enough to exclude the slower rates predicted by prior models (Figure 13). Profiles from near the Macquarie Triple Junction give rates 5–6 mm/yr faster than predicted by prior models and also seem good enough to exclude the predictions of the older models (Figure 12).

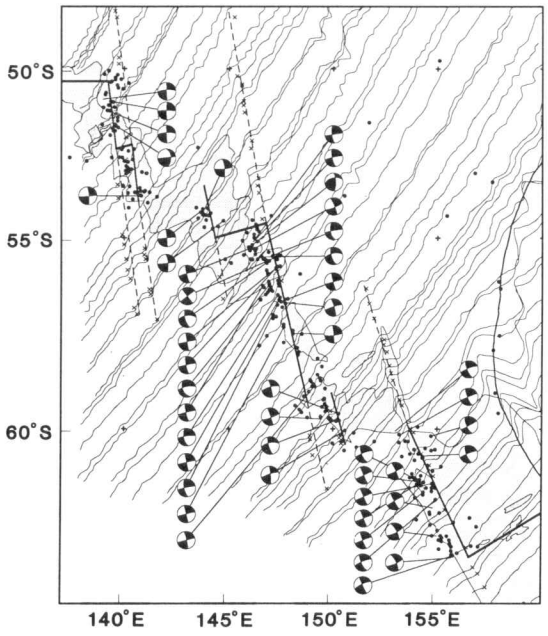

Fig. 15. Geophysical constraints on the trends of the Balleny (155° E), Tasman (147° E), and George V (140° E) transform faults west of the Macquarie Triple Junction. Along-track deflections of the vertical for descending Seasat altimeter passes are used with earthquake epicenters and published bathymetry to locate fracture zones (dashed lines) and transform faults (solid lines). The fracture zone or transform crossing identified from an individual Seasat track is marked with a small cross. The large deflections near 160° E are caused by the Hjort Trench. Seafloor above 2000-m depth is heavily stippled; seafloor between 3000- and 2000-m depth is lightly stippled [*Hayes and Vogel*, 1981]. Only those ridge segments identified from magnetic and bathymetric data are shown. All focal mechanisms are from the CMT solutions; epicenters are from the Earthquake Data File from the NGDC.

Minster and Jordan [1978] and *Stein and Okal* [1978] speculated that a plate boundary dividing the Indian plate from the Australian plate follows the Ninetyeast Ridge and continues southward or southwestward, where it intersects the Southeast Indian Ridge. Seismicity along and near the southern Ninetyeast Ridge might mark the continuation of this boundary (Figure 17). *Stein and Gordon* [1984] used plate motion data to test for this proposed India-Antarctica-Australia Triple Junction and found that the fit of the model to the data improved significantly if a triple junction is located along the Southeast Indian Ridge at ~80°E, near a region of extensive intraplate normal faulting with extension subparallel to the strike of the spreading ridge (Figure 1*a*) [*Bergman et al.*, 1984; *Wiens and Stein*, 1984]. At 26°S, 88°E, *Minster and Jordan's* [1978] model predicts the velocity of the eastern plate relative to the western plate to be 10 mm/yr directed N40°W, similar to the motion estimated by *Stein and Gordon* [1984].

Motion as fast as 10 mm/yr is excluded by the data we present here. Applying *Stein and Gordon's* [1984] method to our data, we found that the fit improved for a hypothetical triple junction near 80°E, but the improvement was insignificant (Figure 18). If the Australian plate is simplistically divided into separate plates west and east of 80°E, the motion of the eastern relative to the western plate is ~2 mm/yr directed ~N20°W at 26°S, 88°E (Figure 17). This is consistent with both the sense of motion expected if the hypothetical boundary is a southward continuation of a left-lateral strike-slip boundary following the northern Ninetyeast Ridge, and the NW-SE shortening suggested by nearby thrust and strike-slip events. However, the predicted motion is inconsistent with the NW-SE extension suggested by the near-ridge focal mechanisms. We conclude that any motion along the southern Ninetyeast Ridge is undetectable with our data and is probably less than 3 mm/yr, a conclusion consistent with the observation that the southern Ninetyeast Ridge and adjacent seafloor are much less seismic than to the north [*Stein and Okal*, 1978; *Bergman and Solomon*, 1985].

The critical test for extension parallel to the strike of the ridge, as suggested by the near-ridge region of intraplate normal faulting, would be to survey the transform

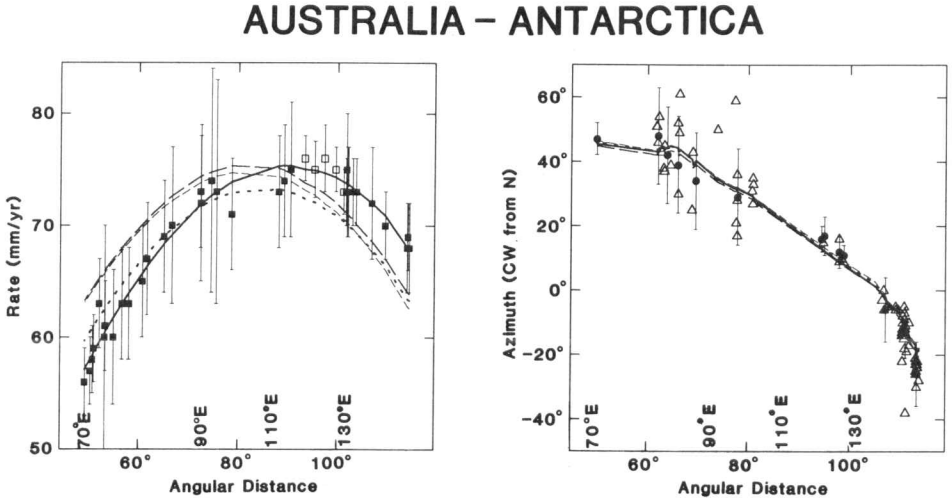

Fig. 16. Australia-Antarctica plate motion data observed along the Southeast Indian Ridge are compared to rates and azimuths calculated from different plate motion models. The horizontal axis shows angular distance from the best fitting Euler vector (Table 2). Squares show seafloor spreading rates (solid when determined from surface magnetic profiles, open when determined from aeromagnetic profiles), circles show observed transform fault azimuths, and triangles show observed slip vector azimuths. The solid line was calculated from our best fitting vector, the long-dashed line from *Chase's* [1978] model, the medium-dashed line from *Minster and Jordan's* [1978] RM2 model, and the short-dashed line from *Tapscott et al.'s* [1980] model. Prior models systematically misfit the observed rates.

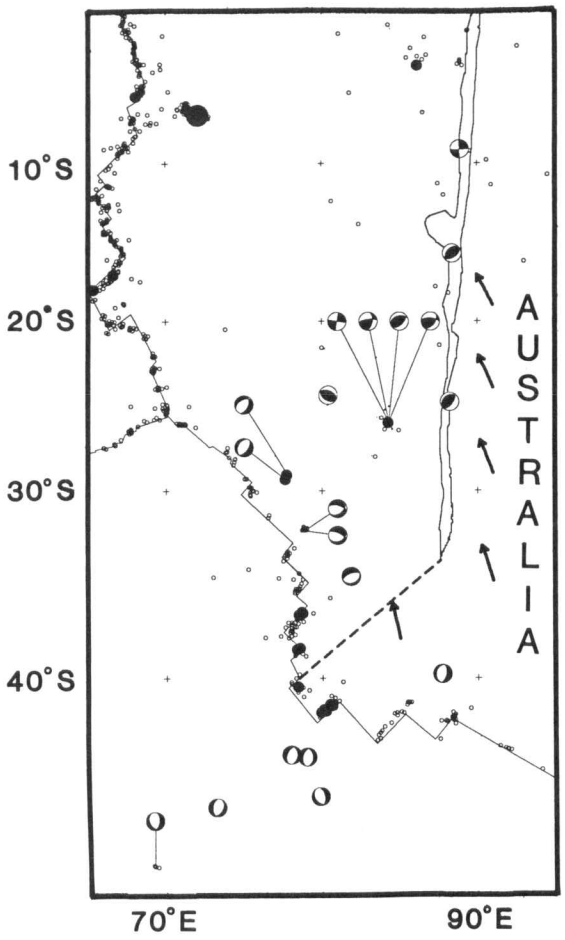

Fig. 17. Seismicity in the southern central Indian Ocean, 1963–1985 (epicenters are from the NGDC). Large solid circles mark earthquakes with magnitude greater than 7.0, medium solid circles mark earthquakes with magnitudes between 5.5 and 7.0, and small open circles mark earthquakes with magnitude less than 5.5. If we assume a hypothetical triple junction exists near 80° E along the Southeast Indian Ridge, we can predict motion of the Australian plate relative to the lithosphere west of the Ninetyeast Ridge. This hypothetical motion is shown by arrows and is about 2 mm/yr directed N20° W. Focal mechanisms are from *Bergman et al.* [1984], *Bergman and Solomon* [1985], *Dziewonski and Woodhouse* [1983], *Dziewonski et al.* [1984*c*, 1986*a*,*b*, 1987*d*, 1988*a*,*b*,*c*].

faults accurately. The present bathymetric data are too sparse and too poor in resolution to show convincing differences in azimuth that could be used to infer deformation of the lithosphere. Detailed surveys of the transform faults using modern seafloor mapping techniques could place strong limits on the rate of extension parallel to the ridge.

Greater deformation is suggested by high values of F east of 135°E, formally significant at the 1% risk level, reflecting a systematic azimuth misfit of ~5° (Figure 18). The azimuths of the transforms east of 135°E (George V, Tasman, and Balleny transforms) and most of the 47 slip vectors from these transforms are CCW of the azimuth determined from the best fitting Euler vector (Figure 16). The systematic misfit of these azimuths has several possible explanations. First, a microplate, bounded to the west by the Southeast Indian Ridge, to the east by the Macquarie ridge complex, and to the north by the 50°S parallel, may move independently of the Australian plate (Figure 19). Second, off-ridge seismicity within this salient part of the Australian plate suggests diffuse intraplate deformation [*Stewart*, 1983] (Figure 19), which might affect the direction of motion along the Southeast Indian Ridge. Third, there may be systematic errors in the estimates of the transform azimuths in the Australia-Antarctic Discordance, east of 135°E, or both.

The first possibility seems unlikely. When we simplistically divided a hypothetical Macquarie microplate from the main Australian plate at 140°E along the Southeast Indian Ridge, ~6 mm/yr west-southwestward motion of the microplate is predicted. The sense of motion is orthogonal to the slip suggested from the one relevant available focal mechanism (Figure 19), frustrating any attempt to define a consistent kinematic model. Thus if the misfits have a tectonic explanation, a pattern of deformation more complex than a simple microplate model is needed.

However, the misfits may require no tectonic explanation. The spreading rates are fit well by the rigid plate model. The misfit transforms are poorly surveyed. Although systematically misfit, none of the transforms are misfit outside the errors we assigned them. The transform

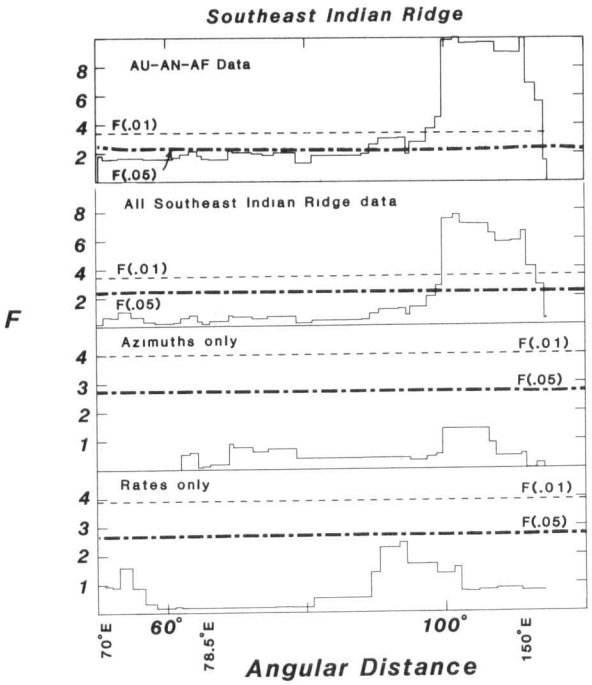

Fig. 18. F versus hypothetical triple junction locations along the Southeast Indian Ridge. The horizontal axis shows angular distance from the best fitting Euler vector (Table 2). The dashed line is the threshold for the 1% risk level, and the dot-dashed line is the threshold for the 5% risk level. The uppermost plot shows the results using all Australia-Antarctica-Africa plate motion data. The plot just beneath it shows the results for all data along the Southeast Indian Ridge and is analogous to Figures 7 (Southwest Indian Ridge) and 10 (Central Indian Ridge). The lower two plots show the azimuth-only and rate-only results for data along the Southeast Indian Ridge. The top two plots show that many locations along the Southeast Indian Ridge east of 135° give formally significant improvements in the fit to the data, if an additional plate boundary is assumed to intersect the Southeast Indian Ridge. However, the bottom two plots suggest this result is not robust and may have a nontectonic explanation.

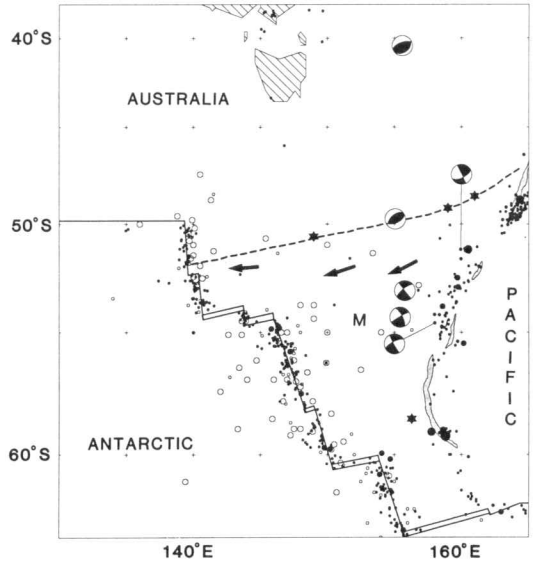

Fig. 19. Seismicity south of Tasmania 1921–1985. Significant off-ridge seismicity within the salient Australian plate lithosphere south of Tasmania includes several historic magnitude 7 events (stars). Other historic events (open circles) have been relocated by *Stewart* [1983]. Focal mechanisms are from *Stewart* [1983], *Dziewonski and Woodhouse* [1983], and *Dziewonski et al.* [1985*d*]. Southeast Indian Ridge plate motion data suggest a plate boundary intersects the ridge between 125° E and 155° E (Figure 18). If a hypothetical Macquarie microplate ("M") is simplistically divided from the main Australian plate at 140° E, ~6-mm/yr west-southwestward motion of the microplate is predicted (arrows in figure). The predicted sense of motion disagrees with the slip suggested from the one focal mechanism available along the hypothetical boundary (dashed line).

azimuths from the Australia-Antarctic Discordance were estimated from offsets of magnetic lineations, a procedure that could lead to a small, systematic bias in the azimuth estimates. If we discard these four azimuths, the significance of the remaining misfits is marginal. Moreover, the few available ship tracks east of 135°E suggest these eastern transforms may be offset by short ridge segments. If true, the azimuths, which are estimated from Seasat transform crossings, sparse bathymetry, and epicenter distributions, may be biased CCW, which could explain the systematic misfits (Figures 16 and 23). Moreover, D. F. Argus et al. (Plate motion, microplates, and closure of the Africa-North America-Eurasia plate circuit, submitted to *Journal of Geophysical Research*, 1988) have shown that slip vectors along accurately mapped North Atlantic transform faults have a CCW bias along left-lateral slipping transforms, which is in the same sense as the misfit between model azimuths and observed slip vector azimuths along the Southeast Indian Ridge.

The statistical significance of the misfit also is not robust. When we apply the test for an additional plate boundary to only the azimuth data, or only the rate data, no significant improvement in fit is found (Figure 18). In light of this, the significance of the improvement in fit to the combined data is questionable. We suspect that the test with the combined data is giving too much weight to the misfit azimuths because the value of reduced chi-square for the rate-only fit is less than half that for the azimuth-only fit. We suspect that the misfit is insignificant.

Thus it seems premature to assume a tectonic cause for the misfit to the azimuths. The best test to distinguish between a tectonic and nontectonic cause of the misfits would be a modern seafloor survey of transform faults along the Southeast Indian Ridge from the Australia-Antarctic Discordance to the Macquarie Triple Junction. A second test is provided by closure of the Australia-Pacific-Antarctic plate circuit. *Minster and Jordan's* [1978] Euler vector describing motion of the Pacific relative to the Indo-Australian plate systematically misfits slip vectors from the Macquarie ridge complex by 15–35°. Moreover, their Euler vector predicts increasing conver-

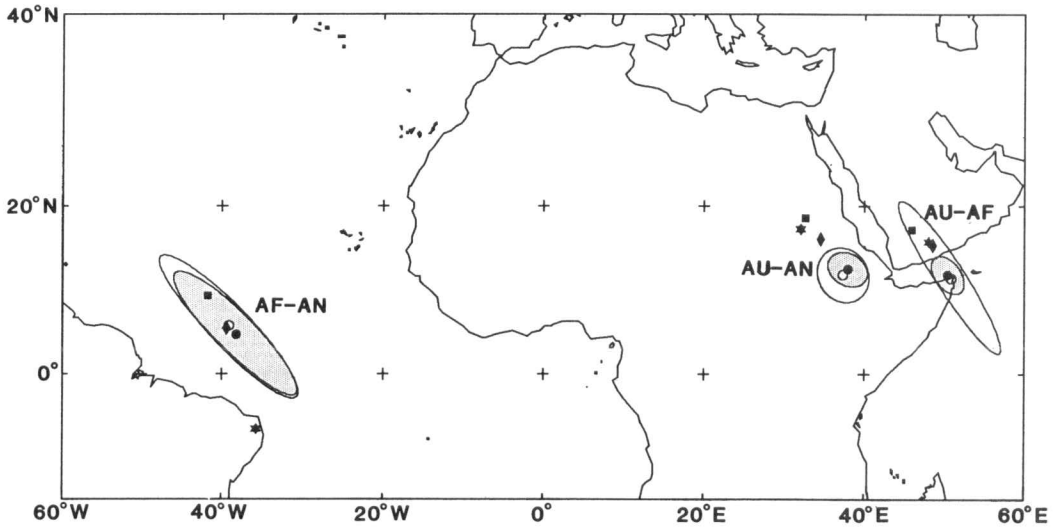

Fig. 20. Australia-Antarctica, Australia-Africa, and Africa-Antarctica Euler poles and 95% confidence limits. The new best fitting poles are shown by open circles; their 95% confidence ellipses are unshaded. The new three-plate poles are shown by solid circles; their 95% confidence ellipses are shaded. Other poles are from *Chase* [1978] (stars), *Minster and Jordan* [1978] (squares), and *Tapscott et al.* [1980] (diamonds).

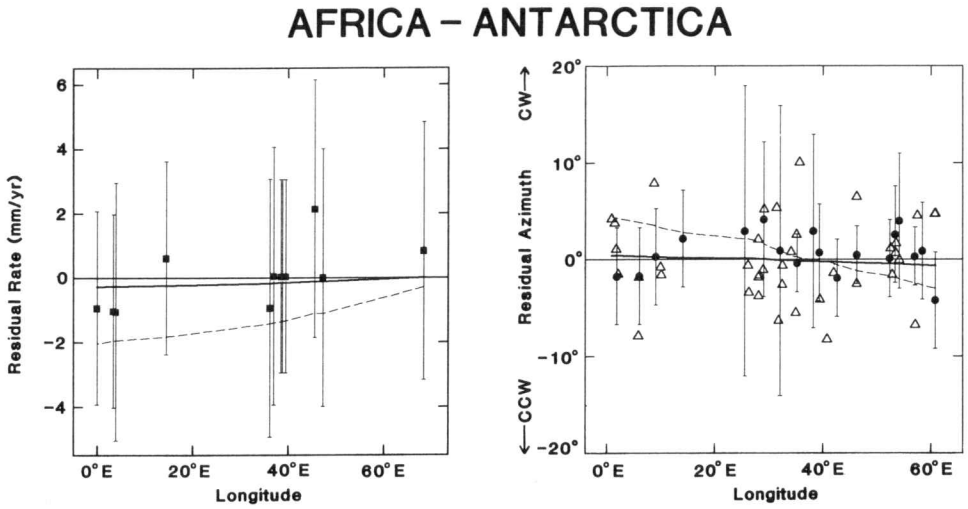

Fig. 21. Africa-Antarctica plate motion data and models shown as residuals relative to rates and azimuths determined from the best fitting Euler vector found in this paper. Squares are seafloor spreading rates determined from surface magnetic profiles, circles are transform fault azimuths, and triangles are slip vector azimuths. The solid line shows rates and azimuths calculated from our closure-enforced three-plate model, and the dashed line shows rates and azimuths calculated from a closure-enforced three-plate model also fit to Carlsberg Ridge data.

gence south along the Macquarie ridge complex. However, south of 60°S, Seasat altimetric data [*Ruff and Cazenave*, 1985] and the transformlike morphology suggest the opposite: predominantly strike-slip motion. Because of the poor fit of Minster and Jordan's model to both their own data and the current Southeast Indian Ridge data, further study will be needed to resolve this question.

In summary, it seems reasonable to use plate motion data along the entire Southeast Indian Ridge in a test of plate circuit closure, while recognizing that good surveys of these transforms may later demonstrate significant misfits.

Three-Plate Model and Plate-Circuit Closure

Our three-plate model gives Euler vectors that exclude prior Australia-Antarctica and Australia-Africa Euler vectors at the 95% confidence level (Figure 20). Unlike prior studies, our closure-consistent three-plate model fits the data nearly as well as they are fit by the separate best fitting vectors (Figures 21–23, Table 2). The value of F computed from (1) is 3.1, which is less than 3.9, the 1% risk level for nonclosure (Figure 24). Thus we find no measurable plate circuit nonclosure. To estimate the smal-

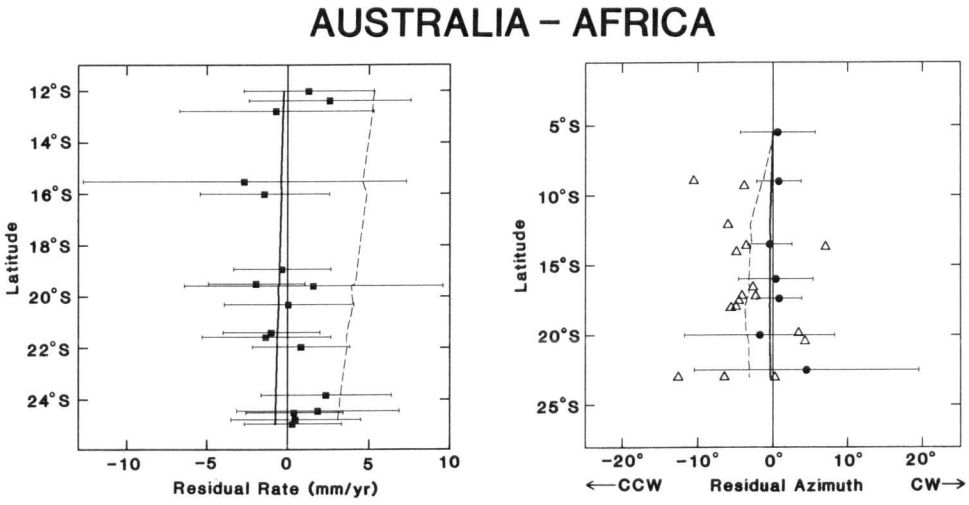

Fig. 22. Australia-Africa plate motion data and models shown as residuals relative to rates and azimuths determined from the best fitting Euler vector found in this paper. Squares are seafloor spreading rates determined from surface magnetic profiles, circles are transform fault azimuths, and triangles are slip vector azimuths. The solid line shows rates and azimuths calculated from our closure-enforced three-plate model, and the dashed line shows rates and azimuths calculated from a closure-enforced three-plate model also fit to Carlsberg Ridge data.

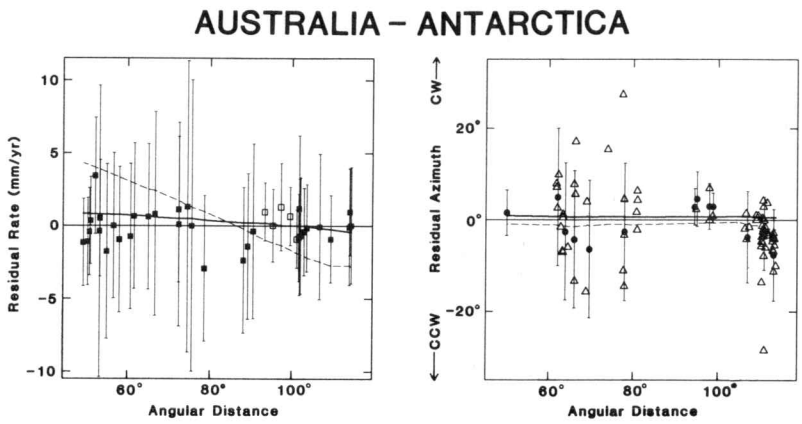

Fig. 23. Australia-Antarctica plate motion data and models shown as residuals relative to rates and azimuths determined from the best fitting Euler vector found in this paper. The horizontal axis shows angular distance from the best fitting Euler vector (Table 2). Squares are seafloor spreading rates (from surface magnetic profiles where solid and from aeromagnetic profiles where open), circles are transform fault azimuths, and triangles are slip vector azimuths. The solid line shows rates and azimuths calculated from our closure-enforced three-plate model, and the dashed line shows rates and azimuths calculated from a closure-enforced three-plate model also fit to Carlsberg Ridge data.

lest deviation from closure we could detect, we used numerical experiments in which we added systematic biases to our data and repeatedly applied the F-ratio test for plate circuit closure. We started with small biases (e.g., adding 1 mm/yr to all rates along a boundary, then testing for closure) and increased the bias in small steps until the F-test showed nonclosure significant at the 1% risk level. These experiments suggest the data are good enough to detect nonrigidity exceeding ~2 mm/yr or ~2° along the Southeast Indian Ridge, ~2 mm/yr or ~3° along the Central Indian Ridge, and ~2 mm/yr or ~10° along the Southwest Indian Ridge.

In a prior analysis using the F-ratio test for plate circuit closure, *Gordon et al.* [1987] found that *Minster and Jordan's* [1978] data failed closure, regardless of the geometry assumed for the Indian plate. Here we find that the data of *Tapscott et al.* [1980] also fail closure at the 1% risk level, which is surprising because they found closure from the same data (Figure 24). However, their Euler vectors differ from the Euler vectors we determined from their data. Apparently *Tapscott et al.* [1980] fit their own data along the Southwest and Central Indian ridges well, but at the cost of misfitting their rates along the Southeast Indian and Carlsberg ridges. When we invert their data excluding the Carlsberg Ridge data, we find consistency with closure (Figure 24).

How would our results have been affected had we assumed, as in nearly all prior studies, that there is a single Indo-Australian plate (Figure 2*a*)? This geometry worsens the fit to data along the three ridges. It causes systematic trends in the misfits to rates from the Southwest and Southeast Indian ridges (Figures 21 and 23), and the azimuths from the Southwest Indian Ridge (Figure 21). It produces a model with Central Indian Ridge rates that are too fast by 3–5 mm/yr (Figure 22). The value of χ^2 is triple that obtained with the revised Indian plate geometry; the test for circuit closure gives F=104, showing nonclosure significant at the 0.00001% risk level. The rates predicted along the Central Indian Ridge and the misfit to rates along the Southeast Indian Ridge are similar to those of prior global models, suggesting that the old model for the plate geometry contributed to the poor fits to Indian Ocean data of prior studies.

Unless we adopted the new plate geometry of *Wiens et al.* [1985], we would not have found closure of the plate circuit. However, some older data sets (e.g., *Minster and Jordan* [1978]) are inconsistent with closure even if the new geometry is adopted (Figure 24) [*Gordon et al.*, 1987].

TABLE 2. Australia-Antarctica-Africa Euler Vectors

Plate Pair	Three-Plate Euler Vector			Best Fit Vector		
	Latitude °N	Longitude °E	ω deg-m.y.$^{-1}$	Latitude °N	Longitude °E	ω deg-m.y.$^{-1}$
AF-AN	4.62	–38.11	0.142	5.93	–39.12	0.142
AU-AN	13.01	37.74	0.679	11.77	37.63	0.678
AU-AF	12.43	50.09	0.657	11.83	50.77	0.678

Euler vectors describe right-handed rotations of the first plate relative to the second. AF is the African plate, AU is the Australia plate, and AN is the Antarctic plate.

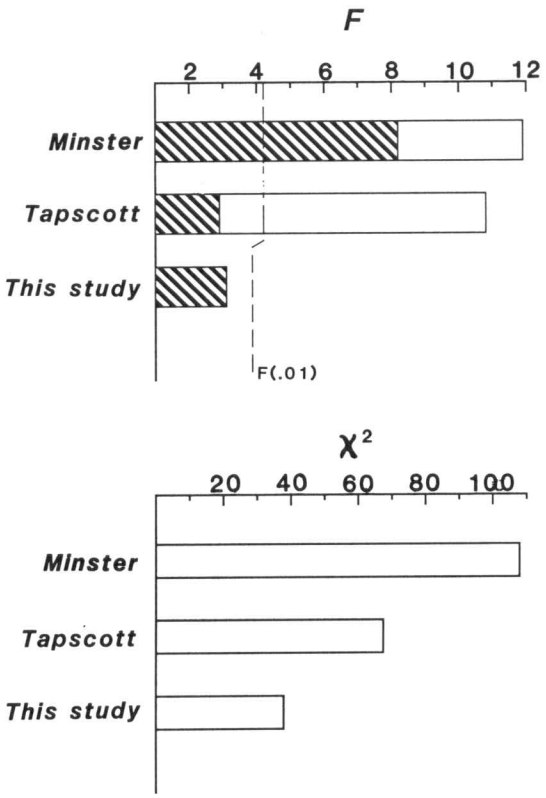

Fig. 24. (Top) Results of the F-ratio test for plate circuit closure applied to the Indian Ocean plate motion data of *Minster and Jordan* [1978], *Tapscott et al.* [1980], and this study. With the plate geometry adopted in prior studies (i.e., including Carlsberg Ridge data in the test), both prior data sets fail closure at a high level of significance (full length of bars, including unshaded portion). If the new plate geometry is used (i.e., Carlsberg Ridge data deleted), the new data set presented here and Tapscott et al.'s data are consistent with plate circuit closure, but Minster and Jordan's data are not. (Bottom) Comparison of the χ^2 fit of successive plate motion models to the new data set presented here. Both prior models fit the new data significantly worse than does the new model presented here. The more recent model of *Tapscott et al.* [1980] gives a better fit than the older model of *Minster and Jordan* [1978].

Therefore the circuit closes only if both the revised geometry and our new data set are used.

Discussion

The most important result here is that motion about the Africa-Australia-Antarctica plate motion circuit is consistent with closure, a result differing from that found by *Minster and Jordan* [1978], *Stein and Gordon* [1984], and *Wiens et al.* [1985]. The result differs because of many new plate motion data that disagree with prior models, our use of a uniform time-averaging interval for all spreading rates, an interpretation of Central Indian Ridge spreading rates that differs from Minster and Jordan's, and our adoption of a new plate geometry in the Indian Ocean. The F-ratio test for plate circuit closure, as well as Figures 9, 16, and 21–23, shows that spreading rates, which were systematically misfit by prior models, are fit well by our model even when closure is enforced. Although many data suggest the Australian plate is deforming, our results suggest that lithospheric deformation outside the equatorial diffuse plate boundary (Figure 2*b*) is no more than a few millimeters per year, which is several times smaller than ~15 mm/yr, the rate of N-S shortening across the equatorial diffuse plate boundary [*Wiens et al.*, 1985].

The conceptual shift from a model with pervasive, intraplate deformation of an Indo-Australian plate to a model with a diffuse boundary between separate rigid plates containing India and Australia is important. A rigid plate model has few adjustable parameters and makes specific predictions, such as predicting the integral of the strain or strain rate across the equatorial zone of deformation. Its usefulness is demonstrated by the excellent fit to 240 data we obtain using only six adjustable parameters. Moreover, the model of two rigid plates is more useful than the intraplate deformation model because the latter implies that self-consistent global models of present-day plate motions will be degraded unless Indian Ocean data are excluded. We thus conclude that a model of intraplate deformation of an Indo-Australian plate is less accurate and less useful than a model in which separate, rigid (or nearly rigid) plates containing India and Australia are divided by a diffuse plate boundary.

Conclusions

The plate motion data along the entire Southwest Indian Ridge show no evidence for motion between Nubia and Somalia, suggesting that any motion near the ridge is small, no more than ~2 mm/yr. Plate motion data along the Southeast Indian Ridge place an upper limit of ~3 mm/yr for possible motion along a plate boundary previously proposed to extend southward or southwestward from the southern Ninetyeast Ridge. With the possible exception of azimuths along the eastern Southeast Indian Ridge, a region warranting further study, all plate motion data are consistent with plate rigidity (and plate circuit closure) to an accuracy of a few millimeters per year. The consistency with closure we find differs from the nonclosure found in prior studies for several reasons including the many new plate motion data that disagree with prior models, our use of a uniform time-averaging interval for all spreading rates, and our use of a new plate geometry in the Indian Ocean. Agreement between model and data shows that lithospheric deformation outside the equatorial diffuse plate boundary (Figure 2*b*) is no more than a few millimeters per year. Thus the Australian plate is, to a good approximation, rigid and can usefully be included in global kinematic models of the motion of rigid plates.

Acknowledgments. Allan Cox influenced the work presented here in many ways. We first learned of the significance and importance of plate rigidity to plate tectonic theory through his writing [*Cox*, 1973], and we learned much of what we know of plate tectonics from prepublication drafts of his textbook [*Cox and Hart*, 1986]. The accurate determination of spreading rates, the most important data analyzed here, would be impossible without the accurate timing of geomagnetic reversals determined by Cox and others. Rates here were determined from the Mammoth Event (reversed) near the center of the Gauss Normal Epoch, both described by *Cox et al.* [1964]. Cox was the Ph.D. thesis advisor, mentor, and friend of one of us (RGG). During a visit to Northwestern's geology department in November 1986, Cox made useful suggestions and encouraged us on the research reported here. We dedicate this paper to his memory.

We thank Emile Okal, Seth Stein, and Dan McKenzie for helpful discussions, Paul Stoddard for use of his map-making programs, Dave Sandwell for sending us GEBCO chart overlays of Seasat data, and Peter Vogt and Dave Wald for sending us enlargements of published and unpublished figures. This research was supported by NSF grant EAR 8417323, NASA grant NAG5-885, and an Alfred P. Sloan Foundation Research Fellowship.

References

Banghar, A. R., and L. R. Sykes, Focal mechanisms of earthquakes in the Indian Ocean and adjacent regions, *J. Geophys Res., 74,* 632–649, 1969.

Bergh, H. W., and I. O. Norton, Prince Edward fracture zone and the evolution of the Mozambique Basin, *J. Geophys. Res., 81,* 5221–5239, 1976.

Bergman, E. A., Intraplate earthquakes and the state of stress in oceanic lithosphere, *Tectonophysics, 132,* 1–35, 1986.

Bergman, E. A., and S. C. Solomon, Earthquake source mechanisms from body waveform inversion and intraplate tectonics in the northern Indian Ocean, *Phys. Earth Planet. Inter., 40,* 1–23, 1985.

Bergman, E. A., J. L. Nabelek, and S. C. Solomon, An extensive region of off-ridge normal-faulting earthquakes in the southern Indian Ocean, *J. Geophys. Res., 89,* 2425–2443, 1984.

Bevington, P. R., *Data Reduction and Error Analysis for the Physical Sciences,* McGraw-Hill, New York, 1969.

Chase, C. G., The N plate problem of plate tectonics, *Geophys. J. R. Astron. Soc., 29,* 117–122, 1972.

Chase, C. G., Plate kinematics: The Americas, East Africa, and the rest of the world, *Earth Planet. Sci. Lett., 37,* 355–368, 1978.

Collette, B. J., A. P. Slootweg, and W. Twigt, Mid-Atlantic Ridge crest topography between 12° and 15°N, *Earth Planet. Sci. Lett., 42,* 103–120, 1979.

Cox, A., *Plate Tectonics and Geomagnetic Reversals,* 702 pp., W. H. Freeman, San Francisco, Calif., 1973.

Cox, A., and R. G. Gordon, Paleolatitudes determined from paleomagnetic data from vertical cores, *Rev. Geophys., 22,* 47–72, 1984.

Cox, A., and R. B. Hart, *Plate Tectonics: How it Works,* 392 pp., Blackwell Scientific, Palo Alto, Calif., 1986.

Cox, A., R. R. Doell, and G. B. Dalrymple, Reversals of the Earth's magnetic field, *Science, 144,* 1537–1543, 1964.

Dziewonski, A. M., and J. H. Woodhouse, An experiment in systematic study of global seismicity: Centroid-moment tensor solutions for 201 moderate and large earthquakes of 1981, *J. Geophys. Res., 88,* 3247–3271, 1983.

Dziewonski, A. M., J. E. Franzen, and J. H. Woodhouse, Centroid-moment tensor solutions for April–June 1983, *Phys. Earth Planet. Inter., 33,* 243–249, 1983*a*.

Dziewonski, A. M., A. Friedman, D. Giardini, and J. H. Woodhouse, Global seismicity of 1982: centroid-moment tensor solutions for 308 earthquakes, *Phys. Earth Planet. Inter., 33,* 76–90, 1983*b*.

Dziewonski, A. M., J. E. Franzen, and J. H. Woodhouse, Centroid-moment tensor solutions for July–September 1983, *Phys. Earth Planet. Inter., 34,* 1–8, 1984*a*.

Dziewonski, A. M., J. E. Franzen, and J. H. Woodhouse, Centroid-moment tensor solutions for October–December 1983, *Phys. Earth Planet. Inter., 34,* 129–136, 1984*b*.

Dziewonski, A. M., J. E. Franzen, and J. H. Woodhouse, Centroid-moment tensor solutions for January–March 1984, *Phys. Earth Planet. Inter., 34,* 209–219, 1984*c*.

Dziewonski, A. M., J. E. Franzen, and J. H. Woodhouse, Centroid-moment tensor solutions for April–June 1984, *Phys. Earth Planet. Inter., 37,* 87–96, 1985*a*.

Dziewonski, A. M., J. E. Franzen, and J. H. Woodhouse, Centroid-moment tensor solutions for July–September 1984, *Phys. Earth Planet. Inter., 38,* 203–213, 1985*b*.

Dziewonski, A. M., J. E. Franzen, and J. H. Woodhouse, Centroid-moment tensor solutions for October–December 1984, *Phys. Earth Planet. Inter., 39,* 147–156, 1985*c*.

Dziewonski, A. M., J. E. Franzen, and J. H. Woodhouse, Centroid-moment tensor solutions for January–March 1985, *Phys. Earth Planet. Inter., 40,* 249–258, 1985*d*.

Dziewonski, A. M., J. E. Franzen, and J. H. Woodhouse, Centroid-moment tensor solutions for April–June 1985, *Phys. Earth Planet. Inter., 41,* 215–224, 1986*a*.

Dziewonski, A. M., J. E. Franzen, and J. H. Woodhouse, Centroid-moment tensor solutions for July–September 1985, *Phys. Earth Planet. Inter., 42,* 205–214, 1986*b*.

Dziewonski, A. M., J. E. Franzen, and J. H. Woodhouse, Centroid-moment tensor solutions for October–December 1985, *Phys. Earth Planet. Inter., 43,* 185–195, 1986*c*.

Dziewonski, A. M., G. Ekstrom, J. E. Franzen, and J. H. Woodhouse, Centroid-moment tensor solutions for January–March 1986, *Phys. Earth Planet. Inter., 45,* 1–10, 1987*a*.

Dziewonski, A. M., G. Ekstrom, J. E. Franzen, and J. H. Woodhouse, Centroid-moment tensor solutions for April–June 1986, *Phys. Earth Planet. Inter., 45,* 229–239, 1987*b*.

Dziewonski, A. M., G. Ekstrom, J. E. Franzen, and J. H. Woodhouse, Centroid-moment tensor solutions for July–September 1986, *Phys. Earth Planet. Inter., 46,* 305–315, 1987*c*.

Dziewonski, A. M., G. Ekstrom, J. E. Franzen, and J. H. Woodhouse, Global seismicity of 1977: Centroid-moment tensor solutions for 471 earthquakes, *Phys. Earth Planet. Inter., 45,* 11–36, 1987*d*.

Dziewonski, A. M., G. Ekstrom, J. E. Franzen, and J. H. Woodhouse, Global seismicity of 1978: Centroid-moment tensor solutions for 512 earthquakes, *Phys. Earth Planet. Inter., 46,* 316–342, 1987*e*.

Dziewonski, A. M., G. Ekstrom, J. H. Woodhouse, and G. Zwart, Centroid-moment tensor solutions for October–December 1986, *Phys. Earth Planet. Inter., 48,* 5–17, 1987*f*.

Dziewonski, A. M., G. Ekstrom, J. E. Franzen, and J. H. Woodhouse, Global seismicity of 1979: centroid-moment tensor solutions for 524 earthquakes, *Phys. Earth Planet. Inter., 48,* 18–47, 1987g.

Dziewonski, A. M., G. Ekstrom, J. E. Franzen, and J. H. Woodhouse, Global seismicity of 1980: centroid-moment tensor solutions for 515 earthquakes, *Phys. Earth Planet. Inter., 50,* 127–154, 1988a.

Dziewonski, A. M., G. Ekstrom, J. E. Franzen, and J. H. Woodhouse, Global seismicity of 1981: centroid-moment tensor solutions for 542 earthquakes, *Phys. Earth Planet. Inter., 50,* 155–182, 1988b

Dziewonski, A. M., G. Ekstrom, J. H. Woodhouse, and G. Zwart, Centroid-moment tensor solutions for January–March 1987, *Phys. Earth Planet. Inter., 50,* 116–126, 1988c.

Dziewonski, A. M., G. Ekstrom, J. H. Woodhouse, and G. Zwart, Centroid-moment tensor solutions for April–June 1987, *Phys. Earth Planet. Inter., 50,* 215–225, 1988d.

Eittreim, S. L., and J. Ewing, Mid-plate tectonics in the Indian Ocean, *J. Geophys. Res., 77,* 6413–6421, 1972.

Engel, C. G., and R. L. Fisher, Granitic to ultramafic rock complexes of the Indian Ocean ridge system, western Indian Ocean, *Geol. Soc. Am. Bull., 86,* 1553–1578, 1975.

Falconer, R. K. H., The Indian-Antarctic-Pacific Triple Junction, *Earth Planet. Sci. Lett., 17,* 151–158, 1972.

Falconer, R. H. K., and M. Tharp, *General Bathymetric Chart of the Oceans (GEBCO),* Sheet 5.14, Canadian Hydrographic Service, Ottawa, Ont., 1981.

Fisher, R. L., and J. G. Sclater, Tectonic evolution of the Southwest Indian Ocean since the Mid-Cretaceous: Plate motions and stability of the pole of Antarctica/Africa for at least 80 Myr, *Geophys. J. R. Astron. Soc., 73,* 553–576, 1983.

Fisher, R. L., J. G. Sclater, and D. P. McKenzie, Evolution of the central Indian Ridge, western Indian Ocean, *Geol. Soc. Am. Bull., 82,* 553–562, 1971.

Forsyth, D. W., Fault plane solutions and tectonics of the South Atlantic and Scotia Sea, *J. Geophys. Res., 80,* 1429–1443, 1975.

Geller, C. A., J. K. Weissel, and R. N. Anderson, Heat transfer and intraplate deformation in the central Indian Ocean, *J. Geophys. Res., 88,* 1018–1032, 1983.

Gordon, R. G., S. Stein, C. DeMets, and D. F. Argus, Tests for the closure of plate motion circuits, *Geophys. Res. Lett., 14,* 587–590, 1987.

Gutenberg, B., and C. F. Richter, *Seismicity of the Earth and Associated Phenomena* (2nd ed.), Princeton University Press, Princeton, N.J., 1954.

Harland, W. B., A. V. Cox, P. G. Llewellyn, C. A. G. Pickton, A.

G. Smith, and R. Walters, *A Geologic Time Scale,* 131 pp., Cambridge University Press, New York, 1982.

Hayes, D. E., and J. R. Conolly, Morphology of the southeast Indian Ocean, in *Antarctic Oceanology II: The Australian-New Zealand Sector, Antarctic Res. Ser. 19,* edited by D. E. Hayes, pp. 125–145, AGU, Washington, D. C., 1972.

Hayes, D. E., and M. Vogel, *General Bathymetric Chart of the Oceans (GEBCO),* Sheet 5.18, Canadian Hydrographic Service, Ottawa, Ont., 1981.

Macdonald, K. C., The crest of the Mid-Atlantic Ridge: Models for crustal generation processes and tectonics, in *The Geology of North America, vol. M, The Western North Atlantic Region,* edited by P. R. Vogt and B. E. Tucholke, Geological Society of America, Boulder, Colo., 1986.

McAdoo, D. C., and D. T. Sandwell, Folding of oceanic lithosphere, *J. Geophys. Res., 90,* 8563–8569, 1985.

McKenzie, D. P., and J. G. Sclater, The evolution of the Indian Ocean since the late Cretaceous, *Geophys. J. R. Astron. Soc., 24,* 437–528, 1971.

Minster, J. B., and T. H. Jordan, Present-day plate motions, *J. Geophys. Res., 83,* 5331–5354, 1978.

Minster, J. B., T. H. Jordan, P. Molnar, and E. Haines, Numerical modeling of instantaneous plate tectonics, *Geophys. J. R. Astron. Soc., 36,* 541–576, 1974.

Norton, I. O., The present relative motion between Africa and Antarctica, *Earth Planet. Sci. Lett., 33,* 219–230, 1976.

Okal, E. A., and S. Stein, The 1942 southwest Indian Ocean Ridge earthquake: Largest ever recorded on an oceanic transform, *Geophys. Res. Lett., 14,* 147–150, 1987.

Rona, P. A., and D. F. Gray, Structural behavior of fracture zones symmetric and asymmetric about a spreading axis: Mid-Atlantic Ridge (latitude 23°N to 27°N), *Geol. Soc. Am. Bull., 91,* 485–495, 1980.

Royer, J., P. Patriat, R. Fisher, H. Bergh, J. Sclater, and C. Scotese, Tectonic evolution of the Southwest Indian Ridge in the vicinity of the Prince Edward Fracture Zone (abstract), Texas A&M, Geodynamics Symposium, College Station, 1986.

Ruff, L., and A. Cazenave, Seasat geoid anomalies and the Macquarie ridge complex, *Phys. Earth Planet. Inter., 38,* 59–69, 1985.

Sandwell, D. T., Along track deflection of the vertical from Seasat: GEBCO overlays, *NOAA Tech. Memo, NOS NGS-40,* 1984.

Schlich, R., The Indian Ocean: Aseismic ridges, spreading centers, and oceanic basins, in *The Ocean Basins and Margins, 6, The Indian Ocean,* edited by A. E. N. Nairn and F. G Stehli, pp. 51–147, Plenum, New York, 1982.

Schlich, R., and P. Patriat, Mise en evidence d'anomalies magnetiques axiales sur la branche ouest de la dorsale mediо-indienne, *C. R. Acad. Sci., 272,* 700–703, 1971.

Schouten, H., and K. McCamy, Filtering marine magnetic anomalies, *J. Geophys. Res., 77,* 7089–7099, 1972.

Sclater, J. G., C. Bowin, R. Hey, H. Hoskins, J. Peirce, J. Phillips, and C. Tapscott, The Bouvet Triple Junction, *J. Geophys. Res., 81,* 1857–1869, 1976*a*.

Sclater, J. G., B. P. Luyendyk, and L. Meinke, Magnetic lineations in the southern part of the Central Indian Basin, *Geol. Soc. Am. Bull., 87,* 371–378, 1976*b*.

Sclater, J. G., H. Dick, I. O. Norton, and D. Woodroffe, Tectonic structure and petrology of the Antarctic plate boundary near the Bouvet Triple Junction, *Earth Planet. Sci. Lett., 37,* 393–400, 1978.

Sclater, J. G., R. L. Fisher, P. Patriat, C. Tapscott, and B. Parsons, Eocene to recent development of the South-west Indian Ridge, a consequence of the evolution of the Indian Ocean Triple Junction, *Geophys. J. R. Astron. Soc., 64,* 587–604, 1981.

Scott, D. R., and H. Kanamori, On the consistency of moment tensor source mechanisms with first-motion data, *Phys. Earth Planet. Inter., 37,* 97–107, 1985.

Searle, R. C., GLORIA investigations of oceanic fracture zones: comparative study of the transform fault zone, *J. Geol. Soc. London, 143,* 743–756, 1986.

Searle, R. C., and A. S. Laughton, Sonar studies of the Mid-Atlantic Ridge and Kurchatov fracture zone, *J. Geophys. Res., 82,* 5313–5328, 1977.

Spiegel, M. R., *Schaum's Outline of Theory and Problems of Probability and Statistics,* 372 pp., McGraw-Hill, New York, 1975.

Stein, S., and R. G. Gordon, Statistical tests for additional plate boundaries from plate motion inversions, *Earth Planet. Sci. Lett., 69,* 401–412, 1984.

Stein, S., and E. A. Okal, Seismicity and tectonics of the Ninetyeast Ridge area: Evidence for internal deformation of the Indian plate, *J. Geophys. Res., 83,* 2233–2245, 1978.

Stewart, L. M., Strain release along oceanic transform faults, Ph. D. thesis, Yale Univ., New Haven, Conn., 1983.

Sykes, L. R., Seismicity of the Indian Ocean and a possible nascent island arc between Ceylon and Australia, *J. Geophys. Res., 75,* 5041–5055, 1970.

Tapscott, C., P. Patriat, R. L. Fisher, J. G. Sclater, H. Hoskins, and B. Parsons, The Indian Ocean Triple Junction, *J. Geophys. Res., 85,* 4723–4739, 1980.

Vogt, P. R., N. Z. Cherkis, and G. A. Morgan, Project Investigator-I: Evolution of the Australia-Antarctic Discordance deduced from a detailed aeromagnetic study, in *Antarctic Earth Science,* edited by R. L. Oliver, P. R. James and J. B. Jago, pp. 608–613, Australian Academy of Sciences, Canberra, 1983.

Wald, D. J., A seismically active section of the Southwest Indian Ridge, M.S. thesis, Univ. of Ariz., Tucson, 1986.

Wald, D. J., and T. C. Wallace, A seismically active segment of the Southwest Indian Ridge, *Geophys. Res. Lett., 13,* 1003–1006, 1986.

Weissel, J. K., and D. E. Hayes, Magnetic anomalies in the southeast Indian Ocean, in *Antarctic Oceanology II: The Australian-New Zealand Sector, Antarctic Res. Ser. 19,* edited by D. E. Hayes, pp. 165–196, AGU, Washington, D. C., 1972.

Weissel, J. K., R. N. Anderson, and C. A. Geller, Deformation of the Indo-Australian plate, *Nature, 287,* 284–291, 1980.

Wiens, D. A., Historical seismicity near Chagos: A complex deformation zone in the equatorial Indian Ocean, *Earth Planet. Sci. Lett., 76,* 350–360, 1986.

Wiens, D. A., and S. Stein, Intraplate seismicity and stresses in young oceanic lithosphere, *J. Geophys. Res., 89,* 11,442–11,464, 1984.

Wiens, D. A., C. DeMets, R. G. Gordon, S. Stein, D. Argus, J. F. Engeln, P. Lundgren, D. Quible, C. Stein, S. Weinstein, and D. F. Woods, A diffuse plate boundary model for Indian Ocean tectonics, *Geophys. Res. Lett., 12,* 429–432, 1985.

Wilson, J. T., A new class of faults and their bearing on continental drift, *Nature, 207,* 343–347, 1965.

Zuber, M. T., Compression of oceanic lithosphere: An analysis of intraplate deformation in the Central Indian Basin, *J. Geophys. Res., 92,* 4817–4826, 1987.

D. F. Argus and R. G. Gordon, Department of Geological Sciences, Northwestern University, Evanston, IL 60208.

C. DeMets, Naval Research Laboratory, Code 5110, Washington, DC 20375.

(Received November 4, 1987;
revised April 1, 1988;
accepted April 15, 1988.)